

Internal Report ITeSRE/CNR 270/2000

March 2000

**CONSTRUCTION OF A DATABASE
OF CMB SPECTRUM OBSERVATIONS**

R. SALVATERRA AND C. BURIGANA

Istituto TeSRE/CNR, via P. Gobetti 101, I-40129 Bologna, Italy

March 2000

CONSTRUCTION OF A DATABASE OF CMB SPECTRUM OBSERVATIONS

R. SALVATERRA AND C. BURIGANA

Istituto TeSRE/CNR, via P. Gobetti 101, I-40129 Bologna, Italy

SUMMARY – We present the complete set of the measures of the CMB absolute temperature on the basis on the works published in the literature, recognize the main causes of error with the aim of estimating separately the magnitude of the systematic and statistical errors, by focussing in particular on the most recent observations. The main purpose of this work is to create a complete and reasoned database of CMB absolute temperatures. The simple database format permits a reading of the data through any text editor or through programs for data handling. This is the first step for a statistical analysis of CMB spectrum data and their comparison with the theoretical predictions for the distorted spectra in order to derive constraints on physical processes at very high redshifts.

1 Introduction

Since the first observation of the Cosmic Microwave Background (CMB) by Penzias & Wilson (1965), many observations have been made to measure the CMB absolute temperature both at high and low frequencies. The most precise values are given by the FIRAS instrument aboard the COBE satellite (Mather et al. 1999).

In this work we present the complete data of the measurements of the CMB absolute temperature. We linger in particular on the most recent observations, and thus obtaining a critical database of the measures. We analyse the papers in the literature to recognize the main causes of error and to evaluate separately the magnitude of the systematical and statistical errors. As well known, the CMB spectrum provides significant informations on physical processes in the universe at very high redshifts (e.g. Danese & Burigana 1993 and references therein). The construction of a complete and manageable database is a first step for a versatile statistical analysis of CMB spectrum data and their comparison with the theoretical predictions for the distorted spectra.

For the following discussion, the whole set of the CMB spectrum observations has been divided in five sections corresponding to different frequencies ranges. Separately, we analyse the measures of the CMB temperature obtained from the molecular observations (section 8) and those by FIRAS and COBRA (section 9). This division in frequency ranges is mainly related to the different problems which dominate the determination of the CMB temperature at different frequencies:

1. $0.408 < \nu < 1.0$ GHz (section 3), where the uncertainties due to the observation site choice and to the determination of the Galactic contribution dominate;
2. $1.4 < \nu < 2.0$ GHz (section 4), where the uncertainty on the Galactic temperature dominates;
3. $2.3 < \nu < 9.4$ GHz (section 5), where, whilst the Galactic contribution decreases, the uncertainty on the atmospheric temperature becomes important in the measure of T_{CMB} ;
4. $10 < \nu < 37$ GHz (section 6), where experiments both from ground and from balloons have been made. The last ones allow, observing at an altitude of about 25 km, to reduce the problem of the atmosphere contaminating the measurements from the ground;
5. above 50 (section 7). In this section only the values of the CMB temperature from ground and balloon are reported, without further analyses, since in this range the very accurate results from FIRAS are available.

2 General Arguments

We discuss here some arguments in common to all frequency ranges considered in the following. In the first subsection we briefly refer to the theoretical elements of the blackbody spectrum and define the concepts of thermodynamic, brightness and antenna temperature. In the second subsection we analyse the effect of foreground contamination to the measurements of the CMB absolute temperature. This contamination is present at any frequency and is therefore preferable to analyse it separately. In the individual sections the impact of this contribution is then compared with that introduced by the instrumental noise.

2.1 The Blackbody Spectrum

The CMB is expected to exhibit approximately a thermal blackbody (BB) spectrum. We review here some basic properties of BB spectrum useful for following discussion.

The brightness of a BB spectrum is given by

$$B_\nu = B_{\nu,BB} = \frac{2h\nu^3}{c^2} \eta_{BB},$$

where

$$\eta_{BB} \equiv \frac{1}{\exp(h\nu/kT_{th}) - 1};$$

here ν is the observation frequency, T_{th} the true thermodynamic temperature and c , k and h the speed of light, the Boltzmann and the Planck constants respectively; η is the photon distribution function. The photon energy density, ε , and the photon number density, n , are given by

$$\varepsilon = \frac{8\pi h}{c^3} \int_0^\infty \eta(\nu) \nu^3 d\nu;$$

$$n = \frac{8\pi}{c^3} \int_0^\infty \eta(\nu) \nu^2 d\nu.$$

For a BB spectrum $\eta = \eta_{BB}$ and the thermodynamic temperature, T_{th} , completely determines the energy density, ε , and number density, n , of the photons. For a BB spectrum they are given by

$$\varepsilon_{BB} = aT_{th}^4 = \frac{8\pi^5 k^4}{15c^3 h^3} T_{th}^4$$

$$n_{BB} = \frac{30\zeta(3)a}{\pi^4 k} T_{th}^3,$$

where $\zeta(3)$ is the Riemann Zeta function, $\zeta(3) \simeq 1.20$.

For a generic distribution function $\eta(\nu)$ it is usual to define the *thermodynamic temperature* $T_{th}(\nu)$ at a given frequency ν as the temperature of a BB with the same value of η at that frequency ν :

$$\eta(\nu) = [\exp(h\nu/kT_{th}(\nu)) - 1]^{-1}, \quad (1)$$

or equivalently:

$$T_{th}(\nu) = \frac{h\nu}{k} \frac{1}{\ln\left(\frac{1}{\eta(\nu)} + 1\right)}. \quad (2)$$

If $\eta = \eta_{BB}$ then $T_{th}(\nu)$ is exactly the thermodynamic temperature T_{th} , constant at any frequency. $T_{th}(\nu)$ is often called also *brightness temperature*, $T_{br}(\nu)$.

At low frequencies it is possible to expand η_{BB} in powers of $h\nu/kT$, so obtaining the approximation holding in the so-called Rayleigh-Jeans (RJ) region

$$\eta_{BB,RJ} \simeq \frac{kT}{h\nu} \text{ if } \nu \ll \frac{kT}{h}.$$

For a generic distribution function $\eta(\nu)$ it is defined also the *antenna temperature* $T_a(\nu)$ as the temperature at which a BB in the RJ approximation would have the same η at that frequency ν :

$$\eta(\nu) = \eta_{BB,RJ}(\nu) = \left(\frac{h\nu}{kT_a(\nu)} \right), \quad (3)$$

or equivalently:

$$T_a(\nu) = \frac{h\nu}{k} \eta(\nu). \quad (4)$$

For a BB, in the limit $h\nu/kT \ll 1$ (i.e. $\nu \lesssim 30$ GHz or $\lambda \gtrsim 1$ cm) $T_a(\nu)$ is equivalent to $T_{th}(\nu)$. In general $T_a(\nu)$ is related to $T_{th}(\nu)$ by

$$T_a(\nu) = T_{th}(\nu) \frac{h\nu/kT_{th}(\nu)}{\exp(h\nu/kT_{th}(\nu)) - 1}. \quad (5)$$

$T_a(\nu)$ is frequently called also brightness temperature. In this work we will use always the term brightness temperature as equivalent to the thermodynamic temperature.

2.2 Foregrounds

A relevant issue in the final evaluation of the CMB temperature is represented by the necessity of accurately subtracting from the sky temperature the contributes from the Galaxy and from unresolved extragalactic sources [see equation (11)]. In particular, the Galactic emission is the main error source at low frequencies (see Table 5), although the level its contribution strongly depends on the considered frequency range. Thus, we describe separately the valuation and the impact of the Galactic contribution on the determination of the CMB temperature together with the uncertainty associated to its determination.

At frequencies below ~ 30 GHz, the Galactic emission is due principally to the synchrotron emission and to the thermal bremsstrahlung (free-free). We refer amply in this section to the treatment of Partridge (1995).

The synchrotron emission is due to the interaction between the Cosmic Rays electrons and the Galactic magnetic field. Both the energetic electrons and the magnetic field are largely confined to the disk of our spiral Galaxy, so the synchrotron radiation is also confined to a band around the sky aligned with the plane of the Galaxy. The radio frequency spectrum of synchrotron radiation depends on the energy spectrum of the relativistic electrons which produce it. If the energy spectrum is a power law (see Rybicki & Lightman 1979, Chapter 6)

$$S_{syn}(\nu) \propto \nu^{(1-\alpha_{syn})/2}$$

or

$$T_{a,syn}(\lambda) \propto \lambda^{(\alpha_{syn}+3)/2}. \quad (6)$$

In our Galaxy α_{syn} is close to 2.6, so we have essentially $T_{a,syn}(\nu) \propto \nu^{-2.8}$. We analyse below the spectral index determination.

The second mechanism responsible for the radio emission of the Galaxy is thermal bremsstrahlung. In the regions where the ionized matter is optically thin to microwave radiation, the observed antenna temperature produced by plasma at physical temperature T_{pl} (of about 10^4 K for the ionized regions in our Galaxy) is

$$T_{a,pl} = T_{pl}(1 - e^{-\tau}) \simeq T_{pl}\tau,$$

for small optical depth τ .

To a good approximation, the emission coefficient of ionized matter in the radio regime is proportional to λ^2 . Thus both τ and $T_{a,pl}$ are proportional to λ^2 . A more exact treatment

shows that the exponent of the power law dependence lies close to 2.1 in the microwave region (Partridge 1995).

Synchrotron and bremsstrahlung processes dominate the Galactic emission for all wavelengths above about 3 mm. At shorter wavelengths, and especially in the submillimeter region, a new source of emission takes over, namely thermal emission from warm dust in the Galaxy. The antenna temperature of the warm dust has a strong wavelength dependence, approximately given by the law

$$T_{a,hot} \propto \lambda^\gamma,$$

with γ in the range -1 to -2 . Thus dust emission influences spectral observations of the CMB only at the shortest wavelength, below 1 mm.

In Figure 1 (Platania et al. 1998) the typical spectra of the various sources of the Galactic emission are shown. We note that at $6 > \lambda > 0.07$ cm the Galactic emission is $\leq 1\%$ of the CMB temperature. Thus, we expect to have in this region the more accurate measures of the CMB temperature.

The Galactic signal is estimated using a 408 MHz sky map (Haslam et al. 1982) and a compilation of H_{II} sources at 2.5 GHz. We report in the next discussion the analysis of Bensadoun (Bensadoun et al. 1993).

The 408 MHz map is first corrected for the CMB signal of 2.7 ± 1 K (which allows for the possibility of up to a 1 K spectral distortion at 408 MHz), for the H_{II} and for the extragalactic sources at 408 MHz [see equation (7)]. The adjusted 408 MHz sky map and the H_{II} map are convolved with the measured antenna gain pattern to produce a profile at the declination of each observation. These profiles are then scaled to the frequency of the observation using spectral indices of 2.75 ± 0.15 for the 408 MHz data and 2.10 ± 0.05 for the H_{II} data.

The accuracy of the Galactic model at the observation frequency primarily depends on the accuracy of the 408 MHz map and the accuracy of the spectral index used to scale the map. The Haslam's map is a compilation of four different surveys and has overall errors of ± 3 K in the zero level and $\pm 10\%$ in the gain. At very low frequencies [i.e. 600 MHz (Sironi et al. 1990)], the uncertainty on the Galactic temperature is dominated from the error on the zero level of the 408 MHz map. Above 1 GHz, instead, the largest error in the Galactic signal arises from the uncertainty in the spectral index. A first approximation of the spectral index comes from the the 408 MHz map (Haslam et al. 1982) and the map at 1420 MHz by Reich & Reich (1986), after both have been corrected for the CMB signal. The error on α_{syn} due to the gain and zero level uncertainties on the maps at frequencies ν_1 and ν_2 is

$$\delta\alpha_{syn} = \frac{1}{\ln(\nu_1/\nu_2)} \sqrt{\left(\frac{\delta T_1}{T_1}\right)^2 + \left(\frac{\delta T_2}{T_2}\right)^2},$$

where $\delta T/T$ is the relative error of the maps. The ± 0.5 K zero level error on the 1420 MHz map dominates the uncertainty in α_{syn} . An improvement of this evaluation could come by a better determination of the zero level of the 1420 map (Lawson et al. 1987). Otherwise, one can also estimate the spectral index by comparing differences in the Galactic signal at 408 MHz and at higher frequencies.

Another method for the spectral index valuation consists in producing a temperature-temperature plots. Such plots display as ordinate and an abscissa antenna temperatures measured at two different frequencies on the same region of the sky. The slope of the best fit to the data, m , gives the synchrotron index (Platania et al. 1998):

$$\alpha_{syn} = \frac{\log(m)}{\log(\nu_1/\nu_2)},$$

where ν_1 and ν_2 are the frequencies of the two sets of data.

As best valuation of the spectral index, we report here the average from the analysis of Platania et al. (1998)

$$\alpha_{syn} = 2.76 \pm 0.11$$

Many works discussed here use, however, previous and no so accurate valutations.

In determining the value of the CMB temperature, one must also take into account the contribution of the unresolved extragalactic sources (Sironi et al 1990). This can be described by a power law (Toffolatti & De Zotti 1988)

$$T_{ex} = (23 \pm 3) \left[\frac{\nu(MHz)}{178} \right]^{-2.75 \pm 0.05}. \quad (7)$$

3 Range 0.408-1.0 GHz

The low frequencies measures are due in large part to dated experiments (see Table 1). Also the recent observation (Sironi et al. 1990; Sironi et al. 1991) give large error bars (Table 1), which show no substantial improvement to previous measures.

ν (GHz)	λ (cm)	T_{CMB}^{th} (K)	Reference
0.408	73.5	3.7 ± 1.2	Howell & Shakeshaft 1967, Natura, 216, 753
0.6	50	3.0 ± 1.2	Sironi et al. 1990, Ap.J., 357, 301
0.610	49.1	3.7 ± 1.2	Howell & Shakeshaft 1967, Natura, 216, 7
0.635	47.2	3.0 ± 0.5	Stankevich et al. 1970, Australian J. Phys, 23, 529
0.820	36.6	2.7 ± 1.6	Sironi et al. 1991, Ap.J., 378, 550
1	30	2.5 ± 0.3	Pelyushenko & Stankevich 1969, Sov. Astron., 13, 223

Table 1: Values of the CMB temperature measured at $\nu \leq 1$ GHz

An analysis of the recent experiments, made in the last few years, shows that the large error bars are given from different causes (Table 2) and that these are due to the different choice of the observation site. We note however that the uncertainty on the antenna temperature, T_a , is greater than the ones at higher frequencies.

For experiments in Table 2 the absolute measurement of the CMB are done by comparing the output of a radiometer when looking the sky and when looking at a precisely known calibration blackbody maintained at cryogenic temperature, and by subtracting-out any other non cosmological contribution (Bonelli et al. 1995).

The antenna temperature of the sky T_a is calculated by adding the effective temperature T_{eff} of the blackbody calibrator and the measured difference $\Delta T = G(V_a - V_{cs})$, where V_a and V_{cs} are the signals produced respectively by the sky and by the calibrator and G is the system gain (Bonelli et al. 1995). More precisely (Sironi et al. 1991):

$$T_a = \left[\frac{T_{eff} + \Delta T - rT_r}{1 - r} - T_0(1 - e^{-\tau}) \right] / e^{-\tau}, \quad (8)$$

Temperature (K)	ν (GHz)	
	0.600	0.820
Antenna (T_a)	16.46 ± 0.41	6.7 ± 1.5
Ground ($T_{a,gr}$)	5.35 ± 0.70	0.03 ± 0.05
Atmosphere ($T_{a,atm}$)	1.17 ± 0.30	0.90 ± 0.35
Sun ($T_{a,sun}$)	...	0.08 ± 0.08
Galaxy ($T_{a,gal}$)	6.20 ± 0.86	2.67 ± 0.33
Extragalactic		
Sources ($T_{a,ex}$)	0.81 ± 0.11	0.34 ± 0.07
T_{CMB}^{th}	2.94 ± 1.22	2.7 ± 1.6
Site	Alpe Gera	South Pole
Reference	Sironi et al. 1990	Sironi et al. 1991

Table 2: Values and errors of the recent experiments

where T_r is the temperature of the noise radiated by the system, r is the power reflection coefficient of the antenna, $e^{-\tau}$ the trasmission coefficient of the line (cable plus horn) which brings the signal from the antenna to the receiver and T_0 is the physical temperature of the system.

The ideal cold source is a blackbody with the same sky temperature and the closest approximation of this could be represented by an optically thick absorber inside a dewar filled with liquid helium which fits the antenna mouth (Sironi et al. 1990). At low frequencies, however, that solution cannot be used because of the antenna dimensions. It's used instead a coaxial termination, immersed in liquid helium and coupled to the receiver input via cable. The effective temperature T_{eff} is given then (Sironi et al. 1990):

$$T_{eff} = T_l + (\langle T \rangle - T_l)y + T_r R_c, \quad (9)$$

where T_l is the boiling temperature of the liquid in the dewar, $\langle T \rangle$ is the average temperature of the cable between the termination and the receiver, T_r is the noise temperature radiated by the receiver, y is the power absorption coefficient of the cable, and R_c is the power reflection coefficient of the cable. T_l depends on the ambient pressure p and is well known when p is known. T_r , y e R_c can be measured. Calculating the equation (9) the result is that the effective temperature of the coaxial source is higher than that of the liquid helium.

The most convenient configuration, suggested by equation (8), is the one in which the source is coupled to the receveir through the same antenna which looks at the sky, so that $e^{-\tau} = 1$ (Sironi et al. 1991). That is not possible for the observations at these frequencies because of the antenna size. The error on T_a is also dominated by the uncertainty of $e^{-\tau}$. $e^{-\tau}$ is the product of ϵ_f , ϵ_w and ϵ_c . There are respectively the flaring section coefficient, the antenna waveguide section coefficient and the coaxial components coefficient. At the South Pole (Sironi et al. 1991) because of the severe environmental conditions it's not possible to remeasure ϵ_w at the observing site before the waveguide section is fixed at the antenna throat. The value of ϵ_f is given by the average of the values measured in the laboratory before and after the experiment. There is also an additional uncertainty produced by repeated assembling and disassembling of the waveguide section of the horn. Also with reference to the South Pole experiment (Sironi et al. 1991) an undesired source of uncertainty of statistical type comes from the connectors at the end of the cable, placed between the antenna and the receiver to overcome the stiffness of the lines produced by the low ambient temperature.

Anyway, a simple comparison with observations in higher frequencies shows that the errors

on ΔT and T_{eff} (and through equation 8 on T_a) are increased by the impossibility to fit the antenna mouth with the cold source. Table 3 shows a comparison between the uncertainties of these terms measured in the same observation project. It is evident that the different technological solution used at 2.5 GHz (Sironi et al. 1991) allows to reduce the error bars on ΔT and T_{eff} .

	ν (GHz)		
	0.600	0.820	2.5
ΔT	± 0.28	± 0.39	± 0.01
T_{eff}	± 0.30	± 0.42	± 0.01
Site	Alpe Gera	South Pole	
Reference	Sironi et al. 1990	Sironi et al. 1991	

Table 3: Comparison of the uncertainties on ΔT and T_{eff} expressed in K at 0.60 GHz, 0.82 GHz and 2.5 GHz

From the antenna temperature must be subtracted the not cosmological contributions. There are local and foreground contributions.

The sky temperature, $T_{a,sky}$, is achieved by the subtraction of the local terms from the antenna temperature T_a . More precisely (Sironi et al. 1991):

$$T_{a,sky} = T_a - T_{a,gr} - T_{a,atm} - T_{a,sun}, \quad (10)$$

where $T_{a,gr}$, $T_{a,atm}$, $T_{a,sun}$ are the contributions from the ground around the antenna, the Earth's atmosphere and the Sun, respectively.

$T_{a,gr}$ depend on the observation site (Table 2). This term is calculated by convolving the antenna beam profile with a blackbody radiator at ambient temperature having the shape of the ground visible (i.e., not hidden by screens) from the horn mouth (Sironi et al. 1991). At the South Pole this is not a problem because the ground is flat and the ambient temperature is very low. At Alpe Gera (Sironi et al. 1990), on the contrary, because of the horizon shape, very large screens are necessary to stop the ground radiation, but the screen efficiency is questionable because of the presence of few incumbent peaks which make diffraction of their thermal radiation over the screen edges highly probable but difficult to evaluate and/or cut. Thereafter the big error bars of $T_{a,gr}$ in the experiment at Alpe Gera obtain an explanation (Table 2).

On the contrary the Sun contribution must be taken into account only in the South Pole observations, where is not possible to measure during the night. To reduce $T_{a,sun}$, the radiometers are surrounded on three sides by reflecting screens. The resulting value of $T_{a,sun}$ is calculated taking into account the diffraction of the radiation at the screen edges and the antenna power pattern.

The contribution of the Earth's atmosphere can be obtained in principle by measuring the variation of the antenna temperature when the horn is tilted from zenith angle z_1 to z_2 . At low frequencies, however, the galactic signal overcomes the atmospheric signal by a factor ranging from 3 - 30, depending on the observing direction (Sironi et al. 1990). As a result, the value one finds by scaling data at other frequencies is preferable compared to the directly measured value of $T_{a,atm}$. Below a few GHz, the atmosphere is optically thin, and its emission is dominated by the oxygen content of the air mass above the antenna. Therefore, at a given frequency $T_{a,atm}$ can be scaled from one observing site to another by the ratio of the atmospheric pressure at the two sites. To compare data at different frequencies, the

dependence of $T_{a,atm}$ on ν is necessary (Sironi et al. 1990). Below a few GHz most atmospheric models (i.e., Danese & Partridge 1989) predict a nearly flat spectrum down to about 1 GHz and a decrease somewhere below, although it is not possible to exclude that the spectrum may remain flat down to 500 MHz. Assuming a flat spectrum, we have a value for $T_{a,atm}$. The error bar has been set large enough to be compatible with the models and the observational data at nearby frequencies.

The CMB temperature is obtained by subtracting the foreground contributions from the sky temperature, $T_{a,sky}$:

$$T_{a,CMB}(\nu) = T_{a,sky}(\alpha, \delta, \nu) - T_{a,gal}(\alpha, \delta, \nu) - T_{a,ex}(\nu), \quad (11)$$

where α and δ are the celestial coordinates (Sironi et al. 1990).

Between ~ 0.5 and 1 GHz, none of the three components of $T_{a,sky}$ is negligible. In particular, at 600 MHz outside the galactic plane, one expects the following proportions (Sironi et al. 1990):

$$T_{a,gal} : T_{a,CMB} : T_{a,ex} \simeq 7 : 3 : 1.$$

The methods to determine $T_{a,gal}$ and $T_{a,ex}$ are already described in the subsection (2.2). We only note (Sironi et al. 1990) that in this range of frequencies the uncertainty on $T_{a,gal}$ is dominated from the error on the 408 MHz map (Haslam et al. 1982). Were $T_{a,sky}(408)$ known with the accuracy of 0.9K, the error bars could be reduced by about a factor of 2. In this case, the 1 K uncertainty of $T_{a,CMB}(408)$ would dominate (Sironi et al. 1991).

By subtracting all the non cosmological contributes the antenna temperature of CMB radiation is derived; its error bars are obtained by adding in quadrature the uncertainties on the terms of equations (8), (10) and (11).

Through equation (5) we can turn the antenna temperature to the thermodynamic temperature $T_{th,CMB}$, although the difference between these two is less than 1% at these low frequencies.

4 Range 1.4-2.0 GHz

Many measures in this range are carried out in recent times. One expects that observations in this range are low enough in frequency to allow significant distortions, but high enough that the Galactic signal is still a factor of 3 weaker than the CMB (Bensadoun et al. 1993). Table 4 gives the data in this range, while Table 5 shows a comparison of the recent measures. It can be noted that the main error source derives from the determination of the Galactic temperature.

The experiment consists in comparing the signal from the zenith S_a with one coming from a large, liquid-helium cooled, cold-load calibrator S_{load} whose antenna temperature, $T_{a,load}$, is precisely known. The antenna temperature of the zenith, $T_{a,zenith}$, is

$$T_{a,zenith} = G(S_a - S_{load}) + T_{a,load} - \Delta T_{a,inst} - \Delta T_{a,joint}, \quad (12)$$

where G is the gain calibration coefficient for the radiometer, $S_a - S_{load}$ is the measured signal difference between the zenith and the cold load, $\Delta T_{a,inst}$ is the correction for any changes in the radiometer signal associated with its inversion during the measurement, and $\Delta T_{a,joint}$ is

ν (GHz)	λ (cm)	T_{CMB}^{th} (K)	Reference
1.4	21.3	2.11 ± 0.38	Levin et al. 1988
1.42	21.2	3.2 ± 1.0	Penzias & Wilson, 1967
1.43	21	$2.65_{-0.30}^{+0.33}$	Staggs et al. 1996
1.44	20.9	2.5 ± 0.3	Pelyushenko & Stankevich 1969
1.45	20.7	2.8 ± 0.6	Howell & Shakeshaft 1966
1.47	20.4	2.27 ± 0.19	Bensadoun et al. 1993
2	15	2.5 ± 0.3	Pelyushenko & Stankevich 1969
2	15	2.55 ± 0.14	Bersanelli et al. 1994

Table 4: Values of the CMB temperature at frequencies $1 < \nu \leq 2$ GHz

Temperature (K)	ν (GHz)			
	1.410	1.43	1.47	2
$G(S_a - S_{load})$	-0.06 ± 0.03	...	0.39 ± 0.02	0.17 ± 0.03
Source ($T_{a,load}$)	3.78 ± 0.31	...	3.86 ± 0.03	3.85 ± 0.03
Instruments ($\Delta T_{a,inst}$)	0.0 ± 0.083	0.07 ± 0.02	0.02 ± 0.06	0.07 ± 0.04
Joint ($\Delta T_{a,joint}$)	...	$0.79_{-0.21}^{+0.15}$ ^a	0.025 ± 0.070	...
Atmosphere ($T_{a,atm}$)	0.83 ± 0.10	1.82 ± 0.20	1.08 ± 0.08	1.07 ± 0.07
Galaxy ($T_{a,gal}$)	0.80 ± 0.16	5.23 ± 0.16 ^b	0.82 ± 0.19	0.33 ± 0.10
Ground ($T_{a,gr}$)	0.017 ± 0.008	0.040 ± 0.025	0.06 ± 0.03	0.05 ± 0.04
RFI ($T_{a,RFI}$)	0.0 ± 0.01	0.0 ± 0.01
Sun ($T_{a,sun}$)	< 0.01	< 0.01
T_{CMB}^{th}	2.11 ± 0.38	$2.65_{-0.30}^{+0.33}$	2.26 ± 0.20	2.55 ± 0.14
Sito	White Mountain	West Virginia	WM/SP	South Pole
Reference	Levin, 1988	Staggs, 1996	Bensadoun, 1993	Bersanelli, 1994

Table 5: Values and errors of the recent experiments

^a The reported value is the emission of the system of the waveguide and the joint (Staggs et al. 1996)

^b In this table is reported the value of $T_a - T_{a,gal}$, as given in the work of Staggs et al. (1996)

the differential temperature contribution from the imperfect joint between the antenna and the cold load (Bensadoun et al. 1993).

The cold source calibrator is an optical thick absorber in a LHe-cooled dewar (Smoot et al. 1983), that works like a waveguide fitting the antenna mouth, so that in equation (8) $e^{-\tau}$ becomes $\simeq 1$. Errors in the measure of $T_{a,load}$ are due to the fact that the absorbing material is not infinitely thick and also due to the interface between the radiometer and the dewar. As a result, a small fraction of the power emitted by the radiometer is reflected back into the antenna, contributing to the antenna temperature of the absolute reference load (Levin et al. 1988). In recent experiments (Bensadoun et al. 1993) this effect is minimized. Particularly in the observation of 1988 (Levin et al. 1988) this term contributes in large part to the final error on $T_{a,CMB}$, whereas in recent experiments the uncertainties on $T_{a,load}$ are very low (see Table 5).

As stated above, the difference $G(S_a - S_{load})$ is measured repeatedly during the experiment and then follows a Gaussian parent distribution. The error is based solely on the statistical fluctuations (Levin et al. 1988). This is however smaller compared to systematic errors set, that contaminates the observations. The gain variation does not follow a Gaussian distribution, but in fact shows slow drifts (Levin et al. 1988). The horn emission is neglected.

The instrumental offset term in equation (12) takes in consideration the fact that the radiometer properties can change when it is inverted to observe the cold load (Bensadoun et al. 1993). Changes in the gain δG , the system temperature δT_{sys} , the physical temperature of any loss front-end components δT_R and the reflection δR and the insertion loss δL of each component can contribute to the global instrumental uncertainty ΔT_{inst} . More precisely (Bensadoun et al. 1993):

$$\begin{aligned} \Delta T_{a,inst} \simeq & \delta T_{sys} + \delta T_B R + \delta T_R L - \\ & - \frac{\delta G}{G} [T_{sys} + T_{a,load}(1 - R - L) + T_B R + T_R L] + \\ & + \delta R(T_B - T_{a,load}) + \delta L(T_R - T_{a,load}), \end{aligned}$$

where T_B is the broadcast noise temperature.

To the term $\Delta T_{a,joint}$ in equation (12) contribute the differences in the joints between the antenna horn and the interface plates of the cold load and of the ground screen. $\Delta T_{a,joint}$ is due to the differential emission from within the resistive metal to metal joints, the differential transmission of ambient radiation through the joints and the differential joint reflection. The first two terms carry the larger part of the error on $\Delta T_{a,joint}$ because the test is not performed with a LHe temperature absorber and the value comes out from the test made with the load absorber immersed in liquid nitrogen. The difference in reflection between the antenna-ground screen interface and the antenna-load interface is measured using a network analyzer.

The CMB temperature is obtained by subtracting from the antenna temperature all non cosmological terms:

$$T_{a,CMB} = T_a - T_{a,for} - T_{a,atm} - T_{a,gr} - T_{a,sun} - T_{a,RFI}, \quad (13)$$

where $T_{a,for}$ is the foregrounds contribution, $T_{a,atm}$ is the atmosphere contribution, $T_{a,gr}$ is the ground radiation contribution, $T_{a,sun}$ is the Sun contribution and $T_{a,RFI}$ is the manmade interference contribution.

The foreground term $T_{a,for}$ comes by adding the Galactic radiation $T_{a,gal}$ and the extragalactic source radiation $T_{a,ex}$, formerly discussed in the subsection 2.2. The extragalactic

source contribution is neglected here, because it is small respect to the Galactic component. We note here, that at these frequencies the error on $T_{a,gal}$ is the greatest cause of the uncertainty on $T_{a,CMB}$. The Galactic signal is estimated using a 408 MHz sky map (Haslam et al. 1982), scaled at the observation frequency (Bensadoun et al. 1993). The largest error in the Galactic signal arise from uncertainty in the spectral index α , valued by the difference in the Galactic signal at 408 MHz and at higher frequencies.

$T_{a,gr}$ and $T_{a,sun}$ are described in the subsection above.

$T_{a,RFI}$ is controlled by the continuous monitoring of the man-made interference. This is an important factor in selecting the observation site. In conclusion, this term introduces only a small change and therefore its contribution is negligible (Bensadoun et al. 1993).

It remains only to be analysed the atmospheric contribution. At frequencies below 2 GHz the simple extrapolation from values measured at higher frequencies is favourable rather than a direct measurement (Ajello et al. 1995; Levin et al. 1988; Bensadoun et al. 1993). The atmospheric signal in this range is due to resonant and nonresonant emission by complex of pressure-broadened oxygen lines clustered near $\nu = 60$ GHz. The amplitude of the O_2 emission depends on atmospheric pressure and temperature (Bensadoun et al. 1993). The water vapour is instead negligible. Over the range $1 < \nu < 10$ GHz in the simple, dry atmosphere model of Gordon (1967), the attenuation, α , scales approximately as

$$\alpha = A\gamma \frac{x(1+3x)}{g(1-3x)^2 + x(1-x)^2},$$

where $x = (\nu/\nu_0)^2$, $g = (\gamma/\nu_0)^2$, and A and γ are the pressure- and temperature-dependent amplitude and line width parameters for oxygen. In the extrapolation the effect of the finite beam and the uncertain on the parameter γ has been taken into account. The simple extrapolation from values measured at nearby frequencies agrees well with the empirical atmospheric attenuation model of Danese & Partridge (1989).

The error on $T_{a,atm}(0)$ for this method comes from the accuracy of the measure of p , T and the humidity u of the observation site, from the fluctuations of the atmospheric conditions, from the uncertain on α and from the change of p , T and u if there are obtained from balloon flights (Ajello et al. 1995).

A cross-check of this value comes from a direct measurement of the atmospheric temperature. At around 1.5 GHz, the Galactic background is no longer so overhanging to the atmospheric signal. Two methodes are used to determine $T_{a,atm}(0)$ (Ajello et al. 1995). By the *extinction method* one measures the dependence of the apparent temperature of a bright source on θ , the zenith angle. Then, assuming an effective temperature, the atmospheric temperature at zenith can be obtained. This method produces error bars ranging between 0.02 K below 1 GHz and 0.2 K above 1 GHz and has been used at low frequencies. By the *emission method* one assumes a constant sky signal and measure $\Delta T(\theta_1, \theta_2)$, the variation of the atmospheric noise when the antenna zenith angle goes from θ_1 and θ_2 . We have also

$$T_{a,atm}(0) = \frac{\Delta T(\theta_1, \theta_2)}{\langle f(\theta_1) \rangle - \langle f(\theta_2) \rangle},$$

where ΔT and $f(\theta)$ are averaged over the antenna beam¹. At frequencies ≤ 3.8 GHz the systematic errors dominate (Bersanelli et al. 1995).

Bersanelli et al. (1994) carried out a set of measures at different frequencies. In Table 6 are the values obtained and the extrapolations at 1.47 and 2 GHz. The measured value and that extrapolated at 2 GHz are in good agreement.

¹See section 5 for a more accurate analysis

Frequency (GHz)	Measured (K)	Estrapolated (K)	Year
7.5	1.174 ± 0.064	...	1989
3.8	1.070 ± 0.060	...	1989
2.0	0.989 ± 0.070	1.020 ± 0.070	1991
1.47	...	0.977 ± 0.068	...

Table 6: Comparison between the measured and the estrapolated atmospherical emission (South Pole; Pencil beam value) from Bersanelli et al. (1994)

By subtracting all contributions we derive $T_{a,CMB}$. The error bars are obtained by adding in quadrature the uncertainties on the terms in equation (12) and (13). Through equation (5) we convert $T_{a,CMB}$ to thermodynamic temperature T_{CMB}^{th} , whose error comes from the propagation of errors.

5 Range 2.3-9.4 GHz

In the observations between 2.3 and 9.4 GHz (see Tables 7 and 8) it is clear that the uncertainty on the foreground contribution on the final error decreases when the frequency increases; whilst the error on the atmospheric temperature dominates and represents the major cause of the width of the error bars above 2 GHz. As in other subsections, we analyse here the most recent experiments (Table 8). We note however the value of Stokes et al. (1967) that is in good agreement with the FIRAS results (see 9.1) and that has a very low margin of error.

ν (GHz)	λ (cm)	T_{CMB}^{th} (K)	Reference
2.3	13.1	2.66 ± 0.7	Otoshi & Stelzreid 1975, IEEE Trans on Inst & Meas, 24
2.5	12	2.71 ± 0.21	Sironi et al 1991, Ap.J., 378, 550
3.8	7.9	2.64 ± 0.06	De Amici et al 1991, Ap.J., 381, 341
4.08	7.35	3.5 ± 1.0	Penzias & Wilson, 1965, Ap.J., 142, 419
4.75	6.3	2.70 ± 0.07	Mandolesi et al. 1986, Ap.J., 310, 561
7.5	4.0	2.60 ± 0.07	Kogut et al. 1990, Ap.J., 355, 102
7.5	4.0	2.64 ± 0.06	Levin et al. 1992, Ap.J., 396, 3
9.4	3.2	3.0 ± 0.5	Roll & Wilkinson 1966, PRL, 16, 405
9.4	3.2	$2.69^{+0.16}_{-0.21}$	Stokes et al. 1967, PRL, 19, 1199

Table 7: Values of the CMB temperature at $2.3 \leq \nu \leq 9.4$ GHz

The antenna temperature is obtained by the comparison of the sky signal with the signal of a cold well known load, made by an optical thick absorber inside a dewar cooled with liquid helium, that acts like an overmode waveguide which fits the antenna mouth (Sironi et al. 1991).

The antenna temperature of CMB is given by the subtraction of the non cosmological contributions:

Temperature (K)	ν (GHz)					
	2.5	3.8	4.75	7.5	1988	1989
$G(S_a - S_{load})$...	-0.009 ± 0.008	-0.045 ± 0.013	...	-0.146 ± 0.012	-0.126 ± 0.013
Source ($T_{a,load}$)	3.73 ± 0.15	3.762 ± 0.019	3.682 ± 0.010	3.621 ± 0.009	3.671 ± 0.023	...
Atmosphere ($T_{a,atm}$)	1.155 ± 0.300	1.109 ± 0.060	0.997 ± 0.060	1.083 ± 0.055	1.083 ± 0.059	1.222 ± 0.064
Galaxy ($T_{a,gal}$)	0.118 ± 0.025	0.055 ± 0.015	0.035 ± 0.025	0.010 ± 0.005	0.010 ± 0.005	0.007 ± 0.004
Ground ($T_{a,gr}$)	0.030 ± 0.050	0.006 ± 0.008	0.020 ± 0.010	0.013 ± 0.010	0.013 ± 0.010	0.022 ± 0.015
System (ΔT_{sys})	...	0.034 ± 0.034	0.0 ± 0.020	0.052 ± 0.034	0.052 ± 0.034	0.023 ± 0.025
RFI ($T_{a,RFI}$)	0.0 ± 0.005	...	0.0 ± 0.005
Sun ($T_{a,sun}$)	0.0 ± 0.005
$T_{a,ex}$	0.016 ± 0.005
T_{CMB}^{th}	2.50 ± 0.34	2.64 ± 0.06	2.70 ± 0.07	2.60 ± 0.07	...	2.64 ± 0.06
Site	SP	WM/SP	WM	WM	WM	SP
Reference	Sironi, 1991	De Amici, 1991	Mandolesi, 1986	Kogut, 1990	Levin 1992	

Table 8: Values and errors of the recent experiments

$$T_{a,CMB} = G(S_a - S_{load}) + T_{a,load} - T_{a,gal} - T_{a,atm} - T_{a,gr} - T_{a,RFI} - \delta T_{sys}, \quad (14)$$

where the terms are already explained in section 4. The error bars on $T_{a,CMB}$ is given by adding in quadrature of the uncertainties of the terms in equation (14).

Again, we pass to the thermodynamic temperature through the equation (5).

As far as the non cosmological contributions, we must examine in detail only the atmospheric and system contributions, since the others are already explained in the previous sections (see subsection 2.2 for $T_{a,gal}$ and section 4 for the others).

The term δT_{sys} refers to any systematic change (such as might be caused by gravitational stresses or twisting cables) in the radiometer performance when it is inverted to look at the cold-load calibrator. We have (De Amici et al. 1991):

$$\delta T_{sys} = \delta T_{a,inst} + \frac{\delta G}{G}(T_{a,load} + T_{sys}) + \delta R(T_{sys} - T_{a,load}) + \delta L(T_{phys} - T_{a,load}), \quad (15)$$

where $\delta G/G$ represents the fractional change in calibration coefficient between the upright and the upside down position, δR is the change in reflection coefficient of the horn and amplifier, δL is the change in insertion loss (attenuation of the incoming signal) of the radiometer, T_{phys} is the physical temperature of the components, T_{sys} is the system temperature of the receiver and ΔT_{inst} is the position-dependent change in receiver output. This term is measured (Levin et al. 1982) by 'flip tests', in which a stable target is fixed to the radiometer, which is repeatedly inverted to simulate CMB measurement. It is not possible however to build an invertible liquid helium target; therefore the value of δT_{sys} at this temperature can only be extrapolated from the measurements at higher temperatures. Contributions to δT_{sys} , given from changes in insertion loss or from reflection, should be proportional to the difference between the target and radiometer temperature. Contributions, given by changes in gain, should be proportional to the target temperature plus radiometer system temperature. Electrical effects should be independent of target temperature. The sum, δT_{sys} , therefore, should be linear in the target temperature. The value and the error of δT_{sys} at 2.7 K is calculated minimizing the χ^2 of two-dimensional linear fit.

The evaluation of $T_{a,atm}$ can be obtained through direct measurement and by calculating from the profile (p, T, u). The accuracy of the two methodes is comparable between 2 and 5 GHz, whilst at higher frequencies is preferable a direct measurement (Ajello et al. 1995). We describe here the method of the direct measurement since in the works discussed here this method is used. In particular, we follow the review of Bersanelli et al. (1995) that measure

the atmospheric emission at many frequencies (1.47, 2.0, 3.8, 7.5, 10 and 90 GHz) in three campaigns of White Mountain and two campaigns of South Pole.

For a nonscattering and nonrefracting atmosphere in thermal equilibrium, the equation of transfer for a signal from outside the atmosphere in units of antenna temperature can be written (Waters 1976)

$$T(H_{obs}) = T_{\infty} \exp[-\tau_{\nu}(0, s_{obs})] + \int_0^{s_{obs}} T_{phys}(s') \exp[-\tau_{\nu}(s' - s_{obs})] k_{\nu}(s') ds', \quad (16)$$

where T_{∞} is the antenna temperature of the background signal (in this case emission from the Galaxy, extragalactic sources and the CMB), H_{obs} is the altitude of the observing site, $T_{phys} = c^2 B_{\nu}(T)/2k_B \nu^2$ with $B_{\nu}(T)$ the Planck function and k_B Boltzmann's constant [$T_{phys}(s')$ approaches the physical temperature at s' in the Rayleigh-Jeans approximation] and τ_{ν} and k_{ν} are, respectively, the optical depth and volume attenuation coefficient at frequency ν . The second term in equation (16) is the atmospheric antenna temperature $T_{a,atm}$.

At low frequencies $T_{a,atm}$ is dominated by emission from the O_2 continuum, characterized by the attenuation coefficient (Danese & Partridge 1989):

$$(k_{\nu})_{O_2,c} = \left(1.12 \times 10^{-4} p \theta^2 \frac{\gamma_0}{\gamma_0^2 + \nu^2} + 3.49 \times 10^{-11} p^2 \theta^{2.5} \right) \nu^2 \text{ dBKm}^{-1}, \quad (17)$$

where $\theta = 300/T$ is the relative inverse temperature parameter in K, p is the dry air pressure in kPa and γ_0 is the width parameter for the O_2 continuum in GHz. The latter can be represented as follows:

$$\gamma_0 = a(p + 1.1e)\theta^b, \quad (18)$$

where e is the partial water vapor pressure in kPa; the parameters a in GHz kPa⁻¹ and b , adimensional, determine through equations (17) and (18) the amplitude of the O_2 continuum emission.

At frequencies above ~ 10 GHz, the contribution of water vapor becomes important. In the limit $\tau_{\nu} \ll 1$ from the second term on the right-hand side of equation (16), the atmospheric temperature can be expressed as (Partridge et al. 1984)

$$T_{a,atm}(\nu) = T_{a,O_2}(\nu) + w T_{a,H_2O}(\nu), \quad (19)$$

where w is the precipitable water vapor content in millimeters and the components T_{a,O_2} and T_{a,H_2O} are expressed in K and Kmm⁻¹, respectively. The quantity w is rapidly variable. Simultaneous measurements at two frequencies ν_1 and ν_2 can be used to test the model.

The antenna temperature of the atmosphere, $T_{a,atm}$, is measured with zenith scans in which each radiometer repeatedly observed the sky at a set of zenith angles, Z . In general, observations at two angles Z_1 and Z_2 produce an estimate of $T_{a,atm}$. The measured signal difference, $\Delta S_{Z_1/Z_2}$, is related to the atmospheric antenna temperature at zenith by:

$$T_{a,atm,Z_1/Z_2}(0) \simeq \frac{G \Delta S_{Z_1/Z_2} - \Delta T_{gal,Z_1/Z_2} - \delta T_{Z_1/Z_2}}{\langle f(Z_1) \rangle - \langle f(Z_2) \rangle} \langle f(0) \rangle, \quad (20)$$

where G is the radiometer gain constant, repeatedly measured during the experiment, and

$$\langle f(Z) \rangle = \int f(Z; \theta, \phi) g(\theta, \phi) d\Omega \quad (21)$$

is the convolution of the atmospheric air mass, $f(Z; \theta, \phi)$, with the antenna gain pattern, $g(\theta, \phi)$, when pointing the radiometer at a zenith angle Z . The term $f(Z)$ must take into account the Earth's curvature

$$f(Z) = \frac{1 + r}{(\cos^2 Z + 2r + r^2)^{1/2}},$$

where r is the atmospheric height in units of Earth's radius. For small Z , $f(Z) \simeq \sec(Z)$.

The quantity $\Delta T_{gal, Z_1/Z_2}$ is the differential Galactic background component, which is subtracted based on low-frequency surveys (Haslam et al. 1982). The term $\delta T_{Z_1/Z_2}$ is the resultant of second-order, differential corrections due to ground radiation $\delta T_{gr, Z_1/Z_2}$, angle-correlated instrumental effects $\delta T_{inst, Z_1/Z_2}$, and possible radio-frequency interference (RFI) $\delta T_{RFI, Z_1/Z_2}$:

$$\delta T_{Z_1/Z_2} = \delta T_{gr, Z_1/Z_2} + \delta T_{inst, Z_1/Z_2} + \delta T_{RFI, Z_1/Z_2} + \dots \quad (22)$$

The relative importance of the various sources of uncertainty depends on frequency and site. In particular, at low frequencies the uncertainty is dominated by the subtraction of the large Galactic background through the propagation of the errors of the 408 MHz map (Haslam et al. 1982). In Table 9 we report the values of the main sources of systematic error and an estimation of the statistical error on the measure of $T_{a, atm}$.

Frequency (GHz)	Galaxy (K)	Ground (K)	Instruments (K)	Gain (K)	Pointing (K)	Beam Pattern (K)	Total Systematic (K)	Statistical (K)
1.47	0.171	0.014	0.047 ^b	0.006	0.028	0.032	0.193 ^c	0.027
2.0	0.081	0.014	0.035	0.006	0.014	0.026	0.094	0.014
3.8	0.023	0.035	0.029	0.020	0.005	0.019	0.058	0.004
7.5	0.010	0.041	0.013	0.004	0.007	0.014	0.047	0.037
10	0.019	0.025	...	0.012	0.006	0.025	0.041	0.034
90	< 0.001	0.030	0.009	0.097	0.057	0.006	0.117	0.200

^a The reported values are for pencil beam; at $\nu < 7.5$ GHz from South Pole, the others from White Moutains

^b Extrapolated for a vertical flip set with angle dependence

^c An error of 0.061 K for the RFI emission is considered

Table 9: Values of the main sources of systematic error and an estimation of the statistical error on the measure of $T_{a, atm}$

From the comparison with the model of Danese & Partridge (1989), above described, we note a general consistence between the experimental and the theoretical results.

We report here also the recent result of Mandolesi et al. (1988) who measure the atmospheric temperature at 94 GHz with a balloon, obtaining a value of $T_{a, atm} \simeq 0.015 \pm 0.006$ K at an altitude of $\simeq 38$ Km, in strict agreement with the atmospheric emission models.

6 Range 10-37 GHz

In the range between 10 and 37 GHz (see Table 10) we can distinguish two kinds of observations. In the first case (Kogut et al. 1988 and De Amici et al. 1985) the observations are taken from the ground with instruments like in observations at low frequencies. For these, we refer to the subsection 5 and previous ones where an accurate analysis of problems and errors of this kind of experiments is already given. Other recent observations (Staggs et al. 1996b; Johnson & Wilkinson 1987) are carried out with balloons. Flying at the altitude of about 25 km, the problems due to the atmosphere, that dominate the uncertainty of the ground measures, are reduced.

ν (GHz)	λ (cm)	T_{CMB}^{th} (K)	Reference
10	3.0	2.62 ± 0.058	Kogut et al. 1988, Ap.J., 325, 1
10.7	2.8	2.730 ± 0.014	Staggs et al 1996b, Ap.J., 473, L1
19.0	1.58	$2.78^{+0.12}_{-0.17}$	Stokes et al. 1967, Phys. Rev. Lett., 19, 1199
20	1.5	2.0 ± 0.4	Welch et al 1967, Phys. Rev. Lett., 18, 1068
24.8	1.2	2.783 ± 0.089	Johnson & Wilkinson 1987, Ap.J. Let , 313, L1
31.5	0.95	2.83 ± 0.07	Kogut et al. 1996, Ap.J., 470, 653
32.5	0.924	3.16 ± 0.26	Ewing et al 1967, Phys. Rev. Lett., 19, 1251
33.0	0.909	2.81 ± 0.12	De Amici et al. 1985, Ap. J., 298, 710
35.0	0.856	$2.56^{+0.17}_{-0.22}$	Wilkinson, 1967, Phys. Rev. Lett., 19, 1195
37	0.82	2.9 ± 0.7	Puzanov et al., 1968, Sov. Astr., 11, 905

Table 10: Values of the CMB temperature at $10 \leq \nu \leq 37$ GHz

We analyse here the problems of the balloon experiments. The antenna temperature of the CMB comes from (Johnson & Wilkinson 1987):

$$T_{a,CMB} = G(S_a - S_{load}) + T_{a,load} - T_{a,offset} - T_{a,WND} - T_{a,HRN} - T_{a,for} - T_{a,gr} - T_{a,IGS}, \quad (23)$$

where $T_{a,WND}$ and $T_{a,HRN}$ are the contributions from the window and the horn respectively, $T_{a,for}$ is the sum of the atmosphere contribution and the dipole contribution and $T_{a,IGS}$ is the screen contribution. All other terms are already described in the previous subsections. In Table 10 we find the values of the terms in equation (23) and the relative uncertainties in the two frequency bands of the experiments here considered.

Temperature (K)	ν (GHz)	
	10.7	24.8
$G(S_a - S_{load})$	-0.011 ± 0.001	
Source ($T_{a,load}$)	2.749 ± 0.004	2.870 ± 0.008
Offset ($T_{a,offset}$)	0.007 ± 0.007	...
Horn ($T_{a,HRN}$)	$0.007^{+0.003}_{-0.003}$	0.050 ± 0.012
Window ($T_{a,WND}$)	0.001 ± 0.001	0.036 ± 0.012
Screens ($T_{a,IGS}$)	0.003 ± 0.003	...
Ground ($T_{a,gr}$)	> 0.005	0.004 ± 0.004
Atmosphere ($T_{a,atm}$)	0.003 ± 0.003	0.002 ± 0.002
Galaxy ($T_{a,gal}$)		0.001 ± 0.001
Dipole ($T_{a,dip}$)	0.002 ± 0.002	-0.002 ± 0.001
T_{CMB}^{th}	2.730 ± 0.014	2.783 ± 0.089^a
Reference	Staggs et al. 1996b	Johnson & Wilkinson 1986

Table 11: Values and errors from the balloon's experiments

^a The error is conservative and comes from adding up the errors

The error on T_{CMB}^{th} is abundantly dominated by systematic errors. Statistical errors are considered and include the radiometer noise and the uncertainty on the gain G and on the evaluation of $T_{a,offset}$ (Johnson & Wilkinson 1987).

In the balloon observations the problem of the atmospheric emission is reduced when flying at an altitude of about 25 km. Atmospheric emission is evaluated by fitting pressure models to the observed decrease in the sky temperature during ascent (Johnson & Wilkinson 1987). In regards to the foregrounds emission, the Galactic term is very small at these frequencies. This is extrapolated from the continuum data at 408 MHz (Haslam et al. 1982) using a spectral index of 2.8 ± 0.1 (Staggs et al. 1996b). The data is also corrected for the dipole of the CMB, as observed by COBE (Fixsen et al. 1996). After the subtraction of the atmospheric and foreground effects, the increase in sky temperature, due to the change of the observation angle, is used to constrain the magnitude of the ground radiation. The largest contribution to $T_{a,gr}$ comes from the ground radiation diffracting over the front edge of the ground screen. In principle, radiation from the ground might reflect off the balloon and into the horn antenna, but since the balloon fills only few sr and has small reflectivity, this effect is negligible (Staggs et al. 1996b). The screens limit also the entry into antenna of the spurious signal, but the ambient temperature of the inner ground screen (IGS), which is fixed to the dewar, is near enough to the beam to contribute to the signal (Staggs et al. 1996b). The magnitude of this effect is determined after the flight by lining the inner surface of the inner ground screen with microwave absorber and measuring this lining's contribution to the sky signal. These results are scaled to account for the much lower emissivity of the aluminum relative to the microwave absorber and the reduced effective emissivity of the absorber at low incidence angles. The terms $T_{a,HRN}$ and $T_{a,WND}$ take into account the corrugated horn emission and the window emission respectively. $T_{a,HRN}$ includes the effect of the short waveguide transition coupling the horn to the waveguide switch.

Finally, the value of $T_{a,offset}$ is determined by removing the horn from the dewar and by replacing with a second thermally regulated waveguide load, identical in construction to the reference load (Staggs et al. 1996b). If the radiometer were ideal, when the measured temperature of the two waveguide loads were equal, no differential signal would be observed from the radiometer. Is observed a difference of few mK. Since their origin is not yet certain, errors equal to the magnitudes of the offsets are assigned to their removal.

The results due to the balloon observations are in good agreement with the value of FIRAS (Mather et al. 1999), that is a T_{CMB} temperature of 2.725 ± 0.002 K (95% CL).

7 Above 50 GHz

We report in Table 12 the values of the CMB temperature at frequencies above 50 GHz obtained from ground or from balloon flights (Bersanelli et al. 1990), even if at these frequencies the FIRAS and COBRA's measures are more accurate. Note the value of Schuster et al., in good agreement with the FIRAS measure (Mather et al. 1999). In the subsection 1.8 will be given a short description of the experiments based on the analyse of molecular lines.

8 Measures based on the analyse of the molecular lines

Before the COBE and COBRA's measurements (section 9), molecular absorption line measurements provided some of the most precise values for the CMB temperature. This method has the interesting aspect to represent one of the few methodes able to verify in a direct way

ν (GHz)	λ (cm)	T_{CMB}^{th} (K)	Reference
53	0.57	2.71 ± 0.03	Kogut et al. 1996, Ap.J., 470, 653
83.8	0.358	2.4 ± 0.7	Kislyakov et al. 1971, Sov. Ast., 15, 29
90	0.33	$2.46^{+0.40}_{-0.44}$	Boyton et al. 1968, Phys. Rev. Lett., 21, 462
90	0.33	2.61 ± 0.25	Millea et al. 1971, Phys. Rev. Lett., 26, 919
90	0.33	2.48 ± 0.54	Boynton & Stokes 1974, Nature, 247, 528
90	0.33	2.60 ± 0.09	Bersanelli et al. 1989, Ap.J., 339, 632
90	0.33	2.712 ± 0.020	Schuster et al. UC Berkeley PhD Thesis
90.3	0.332	< 2.97	Bernstein et al. 1990, Ap.J., 362, 107
90	0.33	2.72 ± 0.04	Kogut et al. 1996, Ap.J., 470, 653
154.8	0.194	< 3.02	Bernstein et al. 1990, Ap.J., 362, 107
195.0	0.154	< 2.91	Bernstein et al. 1990, Ap.J., 362, 107
266.4	0.113	< 2.88	Bernstein et al. 1990, Ap.J., 362, 107

Table 12: Values of the CMB temperature at frequencies > 50 GHz. The measures from FIRAS, COBRA and CN molecules are excluded

the homogeneity of the CMB, i.e. the scaling law of the background temperature with the redshift z . The standard Friedman cosmology predicts in fact a simple relationship between the temperature of the CMB radiation and the redshift:

$$T_{CMB}(z) = T_{CMB}(0)(1 + z), \quad (24)$$

where $T_{CMB}(0)$ is the CMB temperature today.

The indirect measure of the CMB temperature through the molecular observation let's us think that it is possible to determine the CMB temperature also at cosmological distances, that is at redshifts higher than 1. The blackbody temperature at higher redshifts can be measured indirectly by using atomic fine-structure transitions in absorbers toward high redshift quasars (Bahcall & Wolf 1968). The first attempt gave an upper limit for the CMB temperature, $T_{CMB} < 45$ K, at $z = 2.309$ from limits on the fine-structure excitation of C II toward PHL 957 (Bahcall et al. 1973). The recent observations use the C I, because the energy separations in its fine-structure levels are smaller compared to other abundant species (such as O I, C II, Si II, N II). The ground term of C I is split into three levels ($J=0, 1, 2$) with $J=0-1$ and $J=1-2$ separations of 23.6 K and 38.9 K (or 0.61 mm and 0.37 mm). C II is another good species to use for the CMB measurements at high redshifts because it has reasonably small energy separation between its fine-structure levels, 91.3 K.

There are several difficulties in carrying out measurements of $T_{CMB}(z)$ with quasar absorbers. First, the ground state C I absorption lines are often weak and difficult to detect in quasar absorbers at high redshift. Second, other non-cosmological sources such as collisions and pumping by UV radiation can also populate the excited fine-structure levels of C I. Thus, the excitation temperature derived is an upper limit to the CMB temperature, unless the local excitation can be estimated. Third, most absorption lines from abundant species such as O I, C II, Si II, N II show strong saturation in their ground state transitions and hence the population ratio of their excited state to the ground state cannot be accurately determined.

The results of the observations using C I and C II are reported in Table 13, while Figure 2 shows the comparison between the measures and the scale-law of equation (24) (solid line).

There are at least three diatomic molecules common in interstellar clouds that have low-

z	T (K)	Molecule	Quasar	Reference
1.776	$< 16a2\sigma$	C I	QSO 1331+170	Meyer et al. 1986, Ap.J., 308, L37
1.776	7.4 ± 0.8	C I	QSO 1331+170	Songaila et al. 1994b, Nature, 371, 43
1.9731	7.9 ± 1.0	C I	QSO 0013-004	Ge et al. 1996, astro-ph/9607145
2.309	$< 45Ka2\sigma$	C II	PHL 957	Bahcall et al. 1973, Ap.J., 182, L95
2.909	$< 13.5Ka2\sigma$	C II	QSO 0636+680	Songaila et al. 1994, Nature, 368, 599
4.3829	$< 19.6Ka3\sigma$	C II	QSO 1202-07	Lu et al. 1995, Preprint

Table 13: Values of the CMB temperature due to the observation of the fine-structure transition of the C I and C II

lying rotational energy states which can be populated by the CMB thermal radiation: CN, CH and CH^+ . We will concentrate on the cyanogen, since measurements of the population ratio in the other two molecules are very difficult.

We will briefly show like it is possible to determine the CMB temperature from the observations of the absorption lines of the interstellar molecules immersed in the CMB thermal radiation by following the approach of Partridge (1995). Let us begin by considering a collection of very simple quantum mechanical systems with just two energy states E_A and E_B , with $E_B < E_A$; these systems could be atoms or molecules. Place them in an oven maintained at temperature T and allow them to reach thermodynamic equilibrium. The ratio of the numbers in the two energy states, n_A and n_B , is then given by the Boltzmann's equation:

$$\frac{n_B}{n_A} = \frac{g_B}{g_A} \exp[(E_A - E_B)/kT], \quad (25)$$

where g_A and g_B are the so-called statistical weights of the two energy states, which can be calculated from their quantum numbers (in the cases we will consider, $g = 2J + 1$). It is easy to see from equation (25) that energy state B will be appreciably populated only if $E_B - E_A \lesssim kT$. More to the point, we see that if g_A and g_B are known, T can be found directly from a measurement of the population ratio.

In the molecules CN we have an energy difference $E_1 - E_0$, corresponding to a wavelength $\lambda = hc/(E_1 - E_0) = 2.64$ mm, and an additional rotational state with $E_2 - E_1 = 2(E_1 - E_0)$, corresponding at a wavelength of 1.32 mm. Thus, measurements of the population ratios n_1/n_0 and n_2/n_1 permit us to determine T_0 at 2.64 and 1.32 mm, respectively. The ratios of statistical weights appearing in equation (25) are $g_1/g_0 = 3$ and $g_2/g_1 = 5/3$, respectively.

The values of the CMB temperature, obtained from the absorption lines of CN, are given in Table 14. They provide one of the few means to verify the homogeneity of the CMB at least on scales of a few hundred parsecs (Crane 1995). Clearly a few hundred parsecs is not an interesting scale cosmologically, but any variations on these scales would be indicative of larger variations on larger scales. It should be possible to measure the CMB temperature in the Magellanic clouds (Crane 1995).

To determine the CMB temperature from the population ratios of the rotational states of CN, the possibility that other processes (i.e. collisions between electrons and the CN molecules) might alter these must be considered (i.e. collisions between electrons and the CN molecules), since these can lead us to overestimate T_0 using equation 1.25 with no correction for such collisional excitation (Partridge 1995). Unfortunately, the magnitude of the required correction depends on the electron density in the interstellar cloud, n_e , and this quantity can

ν (GHz)	λ (cm)	T_{CMB}^{th} (K)	Observed star	Reference
113.6	0.264	2.70 ± 0.04	z Per	Meyer & Jura 1985, Ap.J., 297, 119
113.6	0.264	2.74 ± 0.05	z Oph	Crane et al. 1986, Ap.J., 309, 822
113.6	0.264	2.76 ± 0.07	HD21483	Meyer et al. 1989, Ap.J. Lett., 343, L1
113.6	0.264	$2.796^{+0.014}_{-0.039}$	ζ Oph	Crane et al. 1989, Ap.J., 346, 136
113.6	0.264	2.75 ± 0.04	ζ Per	Kaiser & Wright 1990, Ap.J. Lett., 356, L1
113.6	0.264	2.834 ± 0.085	HD154368	Palazzi et al. 1990, Ap.J., 357, 14
113.6	0.264	2.807 ± 0.025	16 stars	Palazzi et al. 1992, Ap.J., 398, 53
113.6	0.264	$2.279^{+0.023}_{-0.031}$	5 stars	Roth et al. 1993, Ap.J., 413, L67
227.3	0.132	2.656 ± 0.057	5 stars	Roth et al. 1993, Ap.J., 413, L67
227.3	0.132	2.76 ± 0.20	ζ Per	Meyer & Jura 1985, Ap.J., 297, 119
227.3	0.132	$2.75^{+0.24}_{-0.29}$	ζ Oph	Crane et al. 1986, Ap.J., 309, 822
227.3	0.132	2.83 ± 0.09	HD21483	Meyer et al. 1989, Ap.J. Lett., 343, L1
227.3	0.132	2.832 ± 0.072	HD154368	Palazzi et al. 1990, Ap.J., 357, 14

Table 14: Values of the CMB temperature, measured through the molecules CN

vary from cloud to cloud. The values of the correction for the most observed stars are given in Table 15 (Roth et al. 1993).

Star	T_{loc} (K)
ζ Ophiuchi	$0.0^{+0.031}_{-0.0}$
ζ Persei	$0.0^{+0.031}_{-0.0}$
HD 21483	0.075 ± 0.018
HD 27778	0.020 ± 0.020
HD 154368	0.035 ± 0.009

Table 15: Values of the correction due to local excitation for the most observed stars (Roth et al. 1993)

9 Measures from satellite and rocket

9.1 FIRAS

The FIRAS (Far Infrared Absolute Spectrophotometer) instrument aboard the COBE (COsmic Background Explorer) satellite was designed to measure the spectrum of the CMB temperature.

The FIRAS is a polarizing Michelson interferometer. It measures the spectral difference between a 7° patch of sky and an internal blackbody. The symmetric FIRAS optics are differential, with two input and two output ports. One input port receives emission from the sky, defined by a non-imaging concentrator. The other input port receives emission from an internal reference calibrator (emissivity $\simeq 0.98$) with an associated concentrator. Each of the two output beams is split by a dichroic filter into low and high frequency beams, separated at 20 cm^{-1} , feeding four silicon composite bolometer detectors operated simultaneously. An external blackbody calibrator provides the critical absolute calibration. During calibration the sky aperture is completely filled by the external calibrator with an emissivity > 0.99997 ,

calculated and measured. The external calibrator is isothermal to better than 1 mK at 2.7 K according to calculation. The spectrum uncertainty due to the calibrator is approximately 10 parts per million.

The temperature of the two calibrators and associated concentrators are controllable from 2 to 25 K. Redundant thermometers measure the temperatures of these four temperature controlled elements and other infrared emitters such as the moving mirrors, the mechanical structure, and the detector housings. When observing the sky, the spectrometer is operated with its output nearly nulled, by adjusting the internal calibrator temperature. This reduces sensitively the gain errors and instrument drifts.

A first analysis of the FIRAS data was considered by Mather et al. (1990) for measures in the range $1 < \nu < 20 \text{ cm}^{-1}$. The error bars are a conservative valuation of the systematic errors in the calibration algorithm, corresponding to 1% of the spectrum peak intensity. Mather et al. (1990) obtain a temperature of $2.735 \pm 0.060 \text{ K}$ in the range above mentioned.

A more refined analysis of the FIRAS data in the range $2 < \nu < 20 \text{ cm}^{-1}$ was made by Fixsen et al. (1994) and Fixsen et al. (1996), improving the calibration. The bias of some pixels is corrected, the effects of the Cosmic Rays hits on the detector are removed, data with a large number of glitches are dewighted relative to data with few glitches, 320 points in the spectrum are used rather than 256 and the data are destriped after the calibration. Using the calibration method by Fixsen et al. (1994), Mather et al. (1994) derived the absolute temperature of the CMB as $2.726 \pm 0.010 \text{ K}$ (95 % CL), with a conservative systematic uncertainty estimate. They note a discrepancy between the thermometers and the color temperature scale.

A subsequent analysis of FIRAS data has been performed by Fixsen et al. (1996), that obtained a scale temperature of the CMB as 2.728 ± 0.004 (95% CL). They used three ways to determine the CMB temperature from the FIRAS data set:

1. one use the preflight calibration of the external calibrator thermometers, which should be good to the nominal 1 mK accuracy of the calibration specification. This method gives a CMB temperature of $2.730 \pm 0.001 \text{ K}$, with the error entirely dominated by the absolute thermometry calibration error on the external calibrator;
2. one uses the data to determine the temperature scale. One notes the possibility that the high and the low frequency calibration need not agree. The 0.03% frequency uncertainty implies a temperature uncertainty of 0.82 mK. There is an additional 0.3 mK error in determining the color temperature once the frequency scale is set, but as this adds in quadrature it is negligible. The result of this analysis is that the CMB temperature is $2.7255 \pm 0.0009 \text{ K}$;
3. one can also use the CMB itself. If one assumes the dipole is a result of a Doppler shift the shape of the differential spectrum should be dB_ν/dT , where $B_\nu(T)$ is the Planck function. The best fit temperature to the dipole spectrum is a CMB temperature of $2.717 \pm 0.007 \text{ K}$. The uncertainty is dominated by the uncertainty in fitting the Galaxy radiation which modulates the dipole signal which is only 0.1% of the CMB signal in the Rayleigh-Jeans region.

These three methods give results in agreement one each other within three sigma. By combining them, the absolute temperature of the CMB is then $2.728 \pm 0.004 \text{ K}$ (95% CL), entirely dominated by the systematic errors. While this is not a true statistical uncertainty, it quantifies the uncertainty in the result.

The calibrated destriped sky spectra were then fit to four spatial template. One uses the FIRAS data to determine the spectra of the four components. The data $S(\nu; l, b)$, where l, b are Galactic coordinates and ν is frequency, as follows:

$$S(\nu; l, b) = I_0(\nu) + D(l, b)d(\nu) + G_1(l, b)g_1(\nu) + G_2(l, b)g_2(\nu), \quad (26)$$

where the monopole is represented by the spectrum $I_0(\nu)$; the dipole variation is represented by the spatial distribution $D(l, b)$ and the spectrum $d(\nu)$; and the Galactic emission is represented by one or two spatial distributions $G_k(l, b)$ and the corresponding spectra $g_k(\nu)$. The fits is made independently at each frequency, only the spatial variation is assumed.

To make this separation the functions $D(l, b)$ for the dipole and $G_k(l, b)$ for the Galactic emission must be specified. The dipole is $D(l, b) = \cos(\theta)$, where θ is the angle between the observation and the maximum of the dipole, $(l, b) = (264.26^\circ, +48.22^\circ)$ (Smooth et al. 1992).

Five templates have been considered instead for $G(l, b)$:

1. a plane-parallel, $\csc|b|$, distribution;
2. the spatial distribution of the power received in the high frequency FIRAS channel above 25 cm^{-1} . This is used under the assumption that the high frequency radiation is well correlated to the low frequency Galactic radiation;
3. the COBE DIRBE $240 \mu\text{m}$ map, convolved to FIRAS resolution. This has the advantage of being totally independent and low noise but could suffer from beam convolution errors. The DIRBE resolution is $\sim 0.7^\circ$ and the FIRAS resolution is $\sim 7^\circ$;
4. the COBE DIRBE $140 \mu\text{m}$ map, convolved to the FIRAS resolution;
5. the COBE DIRBE $100 \mu\text{m}$ map, convolved to the FIRAS resolution.

For Galaxy templates 2-5 one uses the normalization $\langle G(l, b) \rangle_{|b| > 60^\circ} = 1.074$, the natural normalization of the $\csc|b|$ model. The only effect of the normalization, of course, is to rescale the Galaxy spectrum.

The monopole $I_0(\nu)$ can be fitted by a Planck blackbody spectrum at the temperature T_0 and by a component of astrophysical monopole.

$$I_0 = B_\nu(T_0) + G_0 g(\nu),$$

where $B_\nu(T_0)$ is a blackbody at temperature T_0 and $G_0 g(\nu)$ is a monopole term. This second component is of astrophysical nature and can not be interpreted in terms of variations of T_0 or of presence of Bose-Einstein or comptonization distortions (Fixsen et al. 1996). By comparing the observation with the model, one obtains for each channel a residue, which, added to the scale temperature value of the spectrum, gives the temperature observed by FIRAS in that channel. The value of the residues, the measured uncertainty and the astrophysical monopole are reported in Table 16.

In Table 17 we report the values and the statistical error of the CMB temperature for each channel of FIRAS.

Table 18 shows the results of the fit by Fixsen et al. (1996).

A recent revision of the calibration work has fixed the value of the absolute temperature at 2.725 ± 0.002 (95% CL) (Mather et al. 1999).

9.2 COBRA

The instrument COBRA developed and tested during the 1980s, was launched on 20 January 1990. In launch condition prior to liftoff the skytelescope port is closed by a vacuum door, the inside being at a temperature about 20 K. During the ascent this door was opened at 150-km altitude allowing the observation of deep space; it was closed at 100 km on descent. The apogee was 250 km. In this section we report the analysis of Gush et al. (1990).

COBRA has measured the CMB temperature at $3 < \nu < 16 \text{ cm}^{-1}$ ($90 < \nu < 500 \text{ GHz}$). In Table 19 the values and the errors for each channel are reported, following the Nordberg & Smoot (1998) report.

The idea of the experiment is to compare the sky radiation with the radiation of a blackbody calibrator. The radiation of the sky is directed to one side of a differential polarizing two-beam interferometer of symmetric construction; the second side of the interferometer is illuminated by an identical telescope, terminated, however, by a conical blackbody calibrator. If the spectrum of the sky were thermal, and the temperature matched that of the calibrator, null interferograms would be produced; deviations from a null interferogram would show immediately that distortions of the CMB are present. The calibration of the internal blackbody was made after the launch by filling the sky telescope aperture by an independent blackbody whose emissivity is calculated to be more than 0.999 and whose temperature could be set anywhere in the range 1.8-4.2 K independently of the temperature of the instrument. The discrepancy of the two calibrators is lower than $\pm 5 \text{ mK}$. This is a limit for the accuracy of the measures.

In the frequency region $3 < \nu < 16 \text{ cm}^{-1}$, where the signal-to-noise ratio is high, the rms scatter of the temperature is 9.5 mK, about 0.33% of the mean. The standard deviation of the mean temperature equals 2 mK. Outside of this band the confidence of the temperature measurement is not good. Nevertheless, one can say with considerable certainty that for $20 < \nu < 30 \text{ cm}^{-1}$ the temperature is less than 3 K.

Various factors contribute to uncertainty in the measured value for the mean temperature: 1) the internal calibrator non uniformity [5 mK]; 2) the uncertainties in offset corrections [3 mK]; 3) the possible non cancellation of microphonics which developed during liftoff [2 mK]; 4) the statistical fluctuations in the measured spectrum [2 mK] and 5) the uncertainties due to heating of the sky telescope by temporary coupling to the warm door during liftoff [5 mK].

The mean value of the CMB temperature is also of 2.736 ± 0.017 , where the error is the linear sum of these uncertainties. This value is in good agreement with the measure of FIRAS in the same range (see section 9.1)

10 Our database

Through the analysis of the observing data of the CMB temperature measurements, already presented above, we have built a reasoned database of these values.

The main purpose of this work is to create a complete collection of the measurements easily accessible (Salvaterra 2000). The database is thus an ASCII file. This simple format permits a reading of the data through any text editor or through programs for data handling.

In Figs. 3-5 we give some plots of the data. Fig. 3 shows all measures of the CMB thermodynamic temperature, while in Fig. 4 reports the more recent measurements. In Fig. 5 we show a comparison between the FIRAS data reported by Mather et al. (1994) and the more refined analysis of them by Fixsen et al. (1996).

10.1 The database structure

The database is organized in two distinguished files to make simpler the reading: either in direct mode through a terminal or through a program. We have grouped in the same file all the interesting numerical values so that the reading program can extract them easily without the need for character handling. The second file contains instead varied kinds of notes, not so interesting under the profile of fits or plots production, but necessary to understand the observation problems and to recover other informations. Each data is represented by a catalogue number so that we may read the two files like a single database and we can at any moment associate a value to its reference and notes. The division in two files is therefore motivated only by a reason of simplicity and the database must be considered as a single object.

The values are arranged in the database in increasing order of frequency (or in decreasing wavelength). We prefer this order instead a different layout (i.e. in chronological order) so that the detailed division in frequency ranges given in the above sections, becomes very clear. As far as the measurements with the same observing frequency, these are in chronological order. The FIRAS and COBRA data are, instead, positioned at end of the database: they are organized in two separate blocks with an increasing frequency order. This way, the access is very easy.

Horizontally the database is divided in 18 columns, 10 in the first file with the numerical values and 8 in the second file with notes and references. The first column of both files contains the catalogue number, necessary to determine univocally the data.

So, the numerical values file is divided in 10 columns.

The first one contains the catalogue number; in the second and third we have respectively the observing frequency and wavelength. In the next one the measured value of the CMB thermodynamic temperature is given, while in the 5th e 6th column we report the absolute values of the upper and lower error associated with this measure.

The last four columns deserve a deeper analysis. They are the synthesis of the analysis of the main error sources studied in the previous sections. They present in order the total amount of the statistical uncertainty on the measured value, the amounts related to the two main sources of systematic uncertainty and a flag. Obviously, we have these values only for the works analysed in detail. In all other cases, the database is filled in by assigning the entire error on the measure to statistical sources and zero value to the systematic errors. The last column is a flag that gives an idea of the type of analysis we have made in the measurement. So that we can distinguish clearly accurately, partially or not at all analyzed data. In Table 20 is reported the meaning of the flag value.

The second file presents in its eight columns useful information for the understanding of the values that we give in the first part of the database. The first column permits to identify the data with its catalogue number. The second and the third column give the cause of the two main sources of systematic error that we have analyzed in the first part of the database, showing straightaway which kind of contributes are the major causes of the uncertainty on the measure. If an analysis of the work has not been made, these columns will be obviously empty. In the 4th column is reported the year of the observation. The 5th column gives the observing site because we have realized that the choice of location is very important for reducing the value of the error bars. When the exact site is not known the only given indication is whether the measure is taken from ground or from balloon. Another important indication is in the 6th column that shows which kind of calibrator is used in the measurement. For the CN experiments we report in this column the observed star or the number of the stars used in the measurement.

The presence of a 'N' in the 7th column refers to a larger note contained in another file. In this instance, the catalogue number permits to find immediately the note desired. This report contains what was not possible to include in the database, but anyway very useful. In this file is also presented the flag legend.

The 8th column reports the reference of the published work, where further informations on the experiment can be found.

10.2 The program of data handling

We have the requirement to generate different files with different choices of data for the fit programs. A simple program is also necessary to build through many options the desired data files. We have implemented it in FORTRAN.

To start, the user must give the name of the output file. Then, other inputs, necessary to exploit the FIRAS data, are required. The program asks the FIRAS scala temperature and its uncertainty reminding the user anyway the latest value of Mather et al. (1999). So, a possible improved FIRAS calibration can be easily taken into account in the future by setting the appropriate value.

The program presents then the main menu of the options. Through these, the user can build the output file by considering the required temperature values. The options are expandable when necessary.

The first 8 options follow the above division in frequency ranges. It is also possible to transfer into the output file, as independent blocks, the values obtained in the various analyzed ranges: 0.408-1 GHz, 1-2 GHz, 2.3-9.4 GHz, 10-37 GHz, over 50 GHz (included the measures from the study of the CN molecular), the COBRA data, the FIRAS data. The eighth option transfers all data. The FIRAS data are available with different options, described in the following. For all the others, the program permits to choose whether the data must be written with the total error or only with the statistical error. Then, the program writes the data in the output file and returns at the main menu so that another choice is possible.

The FIRAS data are available with or without the astrophysical monopole. In each case the user can have the data with the total error or with the statistical error. The total error comes by adding in quadrature the statistical error of the single channel with the error on the scala temperature given at the begin of the program by the user. Then, the program writes the data in the output file and returns at the main menu so that another choice is possible.

The next option permits to decide whether to insert or not in the output file each singular data. For each data is given a short informative table that reports the catalogue number, the observation frequency, the measured value of the CMB thermodynamic temperature, the upper and the lower error totals and the statistical error. Furthermore, it is indicated when the data considered is from the analysis of the CN lines, from COBRA or from FIRAS, and the estimate of the statistical error.

The program asks whether to insert the data in the output file and according to the case with which kind of error (total or statistical). All available measurements are considered, thereafter the program, upon closing, reminds the user the name of the output file. Because the run of the data can be long and boring, together with the program we give same useful parameter files that automatically introduce the answers necessary for building new interesting files.

In this way, we have a file with the measures of recent ground experiments, another one with early ground experiments, a third one from the balloon and a fourth one with CN molecular data. When using these files, remember that the error associated to the measures is the total error.

Another option of the program is to transfer in the output file the values obtained in a

certain range of years as requested by the user. As always, it is possible to have the data either with the total error or with the statistical error. Having finished writing the data, the program, upon closing, reminds the user the name of the output file.

The last option permits to exit the program.

11 Conclusions

We have reviewed all the existing measures of the CMB absolute temperature. After a discussion of the main contamination relevant for the whole set of observed frequencies, we have considered in detail the different sources of contamination relevant at the different frequency bands for ground based, balloon and space observations. We have compared the relative weights of statistical and systematic uncertainties, by focussing in particular on the most recent observations. On the basis of this analysis, we have constructed a complete and reasoned database of CMB absolute temperatures, that allows to easily recognize the relevant informations on the different observations. The simple database format permits a reading of the data through any text editor or through programs for data handling. We have then implemented a set of tools in FORTRAN, that allow to easily select the desired set of measures and discriminate between the quoted statistical and systematic errors. This constitutes a the first step for a versatile comparison of the existing data with the theoretical predictions for the distorted spectra in order to derive constraints on physical processes at very high redshifts.

Acknowledgements. It is a pleasure to thank M. Bersanelli, L. Danese, G. De Zotti, N. Mandolesi and G. Palumbo for useful and stimulating discussions.

12 Symbols index

$d(\nu)$ = dipole spectrum; eqn. 26
 $D(l, b)$ = dipole spatial distribution; eqn. 26
 $e^{-\tau}$ = trasmission coefficient of the line; eqn. 8
 E_A (E_B) = energy in the energy state A (B); eqn. 25
 $f(Z; \theta, \phi)$ = atmospheric air mass; eqn. 21
 g_A (g_B) = statistical weight of the energy state A (B); eqn. 25
 $g_k(\nu)$ = Galactic emission spectrum; eqn. 26
 $g(\theta, \phi)$ = antenna gain pattern; eqn. 21
 G = system gain; eqns. 8, 12, 14
 $G_k(l, b)$ = Galactic emission spatial distribution; eqn. 26
 H_{obs} = altitude of the observing site; eqn. 16
 $I_0(\nu)$ = monopole; eqn. 26
 k_B = Boltzmann's constant
 k_ν = volume attenuation coefficient at frequency ν ; eqn. 16
 $(k_\nu)_{O_{2,c}}$ = attenuation coefficient of the O_2 ; eqn. 17
 n_A (n_B) = population in the energy state A (B); eqn. 25
 p = prpressure
 r = power reflection coefficient of the antenna; eqn. 8
 R_c = power reflection coefficient of the cable; eqn. 9
 S_a = signal from the zenith; eqns. 8, 12, 14, 23

S_{load} = signal from the calibrator; eqns. 8, 12, 14, 23
 S_{syn} = synchrotron power
 $\langle T \rangle$ = average temperature of the cable between the termination and the receiver; eqn. 9
 T_0 = physical temperature of the system; eqn. 8
 T_a = antenna temperature; eqns. 8, 10
 $T_{a,atm}$ = atmosphere antenna temperature; eqns. 10, 13, 14, 19
 $T_{a,hot}$ = warm dust antenna temperature
 $T_{a,ex}$ = extragalactic sources antenna temperature; eqn. 11
 $T_{a,for}$ = foreground antenna temperature; eqns. 13, 23
 $T_{a,gal}$ = Galactic antenna temperature; eqns. 11, 14
 $T_{a,gr}$ = ground antenna temperature; eqns. 10, 13, 14, 23
 $T_{a,load}$ = antenna temperature of the calibrator; eqns. 12, 14, 15
 $T_{a,offset}$ = offset antenna temperature; eqn. 23
 $T_{a,pl}$ = antenna temperature produced by plasma
 $T_{a,sky}$ = sky antenna temperature; eqn. 10
 $T_{a,sun}$ = sun antenna temperature; eqns. 10, 13
 $T_{a,syn}$ = synchrotron emission antenna temperature; eqn. 6
 $T_{a,zenith}$ = zenith antenna temperature; eqn. 12
 $T_{a,CMB}$ = CMB antenna temperature; eqns. 11, 13, 14, 23
 T_{a,H_2O} = water vapor antenna temperature; eqn. 19
 $T_{a,HRN}$ = horn antenna temperature; eqn. 23
 $T_{a,IGS}$ = screen antenna temperature; eqn. 23
 $T_{a,WND}$ = window antenna temperature; eqn. 23
 T_{a,O_2} = O_2 emission antenna temperature; eqn. 19
 $T_{a,RFI}$ = manmade interference antenna temperature; eqns. 13, 14
 T_B = broadcast noise temperature
 T_{eff} = effective temperature of the blackbody calibrator; eqns. 8, 9
 T_∞ = antenna temperature of the background signal; eqn. 16
 T_l = boiling temperature of the liquid in the dewar; eqn. 9
 T_{phys} = physical temperature of the components; eqns. 15, 16
 T_{pl} = physical temperature of the plasma
 T_r = noise temperature radiated by the receiver; eqns. 8, 9
 T_{sys} = system temperature; eqn. 15
 T_{CMB}^{th} = CMB thermodynamic temperature
 u = atmospheric humidity
 y = power absorption coefficient of the cable; eqn. 9
 α = linear absorption coefficient or attenuation
 α_{syn} = synchrotron spectral index; eqn. 6.
 γ_0 = width parameter for the O_2 continuum; eqns. 17, 18
 δG = gain change; eqn. 15
 δL = change in the insertion loss; eqn. 15
 δR = change in the reflection coefficient of the horn and amplifier; eqn. 15
 δT_R = change in the physical temperature of any loss front-end components
 δT_{sys} = change in the radiometer performance; eqns. 14, 15
 $\Delta T_{a,inst}$ = position-dependent change in receiver output; eqn. 12
 $\Delta T_{a,joint}$ = differential temperature contribution from the imperfect joint between the antenna and the cold load; eqn. 12
 ϵ_c = coaxial components coefficient
 ϵ_f = flaring section coefficient
 ϵ_w = antenna waveguide section coefficient

τ_ν = optical depth coefficient at frequency ν ; eqn. 16

References

- [1] Ajello C. et al. 1995, Ap. J. Suppl., 96, 643
- [2] Bahcall J.N. & Wolf R.A. 1968, Ap. J., 152, 701
- [3] Bahcall J.N. et al. 1973, Ap.J., 182, L95
- [4] Bensadoun M. et al. 1993, Ap. J., 409, 1
- [5] Bernstein G.M. et al. 1990, Ap. J., 362, 107
- [6] Bersanelli M. et al. 1989, Ap. J., 339, 632
- [7] Bersanelli M. et al. 1994, Ap. J., 424, 517
- [8] Bersanelli M. et al. 1995, Ap. J., 448, 8
- [9] Bonelli G. et al. 1995, Astro. Lett. Comm., 32, 15
- [10] Boyton P.E. et al. 1968, Phys. Rev. Lett., 21, 462
- [11] Boynton R.A. & Stokes R.A. 1974, Nature, 247, 528
- [12] Crane P. et al. 1986, Ap. J., 309, 822
- [13] Crane P. et al. 1989, Ap. J., 346, 136
- [14] Crane P. et al. 1995, Astro. Lett. Comm., 32, 21
- [15] Danese L. & Partridge R.B. 1989, Ap. J., 342, 604
- [16] Danese L. & Burigana C. 1993, in: "Present and Future of the Cosmic Microwave Background", Lecture in Physics, Vol. 429, eds. J.L. Sanz, E. Martinez-Gonzales, L. Cayon, Springer Verlag, Heidelberg (FRG), p. 28
- [17] De Amici G. et al. 1985, Ap. J., 298, 710
- [18] De Amici G. et al. 1991, Ap. J., 381, 341
- [19] Ewing M.S., Burke B.F., Staelin D.M. 1967, Phys. Rev. Lett., 19, 1251
- [20] Fixsen D.J. et al. 1994, Ap. J., 420, 445
- [21] Fixsen D.L. et al. 1996, Ap. J., 473, 576
- [22] Ge J., Bechtold J., Black J.H. 1996, astro-ph/9607145
- [23] Gush H.P. et al. 1990, Phys. Rev. Lett., 65, 5
- [24] Haslam C.G.T. et al. 1982, A&AS, 47, 1
- [25] Howell T.F. & Shakeshaft J.R. 1966, Nature, 210, 1318

- [26] Howell T.F. & Shakeshaft J.R. 1967, *Nature*, 216, 7
- [27] Howell T.F. & Shakeshaft J.R. 1967, *Nature*, 216, 753
- [28] Johnson D.G. & Wilkinson D.T. 1987, *Ap. J. Lett.*, 313, L1
- [29] Kaiser M.E. & Wright E.L. 1990, *Ap. J. Lett.*, 356, L1
- [30] Kislyakov A.G. et al. 1971, *Sov. Ast.*, 15, 29
- [31] Kogut A. et al. 1988, *Ap. J.*, 325, 1
- [32] Kogut A. et al. 1990, *Ap. J.*, 355, 102
- [33] Kogut A. et al. 1996, *Ap. J.*, 470, 653
- [34] Lawson K.D. et al. 1987, *MNRAS*, 225, 307
- [35] Levin S.M. et al. 1988, *Ap. J.*, 334, 14
- [36] Levin S.M. et al. 1992, *Ap. J.*, 396, 3
- [37] Lu et al. 1995, Preprint
- [38] Mandolesi N. et al. 1986, *Ap. J.*, 310, 561
- [39] Mandolesi N. et al. 1998, *J. Atm. Sol. Terr. Phys.*, Vol. 60, No. 1, 71
- [40] Mather J.C. et al. 1990, *Ap. J.*, 354, L37
- [41] Mather J.C. et al. 1994, *Ap. J.*, 420, 439
- [42] Mather J.C. et al. 1999, *Ap. J.*, 512, 511
- [43] Meyer D.M. & Jura M. 1985, *Ap. J.*, 297, 119
- [44] Meyer D.M. et al. 1986, *Ap. J.*, 308, L37
- [45] Meyer D.M. et al. 1989, *Ap. J. Lett.*, 343, L1
- [46] Millea M.F. et al. 1971, *Phys. Rev. Lett.*, 26, 919
- [47] Nordberg H.P. & Smoot G.F. 1998, *astro-ph/9805123*
- [48] Otoshi & Stelzreid 1975, *IEEE Trans on Inst & Meas*, 24
- [49] Palazzi E. et al. 1990, *Ap. J.*, 357, 14
- [50] Palazzi E. et al. 1992, *Ap. J.*, 398, 53
- [51] Partridge R.B. 1995, '3K: The Cosmic Microwave Background Radiation' Cambridge University Press
- [52] Peebles P.J.E. 1993, 'Principles of Physical Cosmology' Princeton University Press
- [53] Pelyushenko S.A. & Stankevich K.S. 1969, *Sov. Astr.*, 13, 223
- [54] Penzias A.A. & Wilson R.W. 1965, *Ap. J.*, 142, 419
- [55] Penzias A.A. & Wilson R.W. 1967, *Ap. J.*, 72, 315

- [56] Platania P. et al. 1998, Ap. J., 505, 473
- [57] Puzanov V.I., Salomonovich A.E., Stankevich K.S. 1968, Sov. Astr., 11, 905
- [58] Reich P. & Reich W. 1986, A&AS, 63, 205
- [59] Rybicki G.B. & Lightman A.P. 1979, 'Radiative Processes in Astrophysics' A Wiley-Interscience Publication
- [60] Roll P.G. & Wilkinson D.T. 1966, Phys. Rev. Lett., 16, 405
- [61] Roth K.C. 1995, Astro. Lett. Comm., 32, 21
- [62] Roth K.C. et al. 1993, Ap. J., 413, L67
- [63] Salvaterra R., 2000, Degree Thesis, Bologna University
- [64] Schuster et al. UC Berkeley PhD Thesis
- [65] Sironi G. et al. 1990, Ap. J., 357, 301
- [66] Sironi G. et al. 1991, Ap. J., 378, 550
- [67] Smoot G.F. 1997, astro-ph/9705101
- [68] Smoot G.F. et al. 1983, Phys. Rev. Lett., 51, 1099
- [69] Smoot G.F. et al. 1992, Ap. J., 396, L1
- [70] Songaila A. et al. 1994, Nature, 368, 599
- [71] Songaila A. et al. 1994b, Nature, 371, 43
- [72] Staggs S. et al. 1996, Ap. J., 458, 407
- [73] Staggs S. et al. 1996b, Ap. J., 473, L1
- [74] Stankevich K.S. et al. 1970, Australian J. Phys., 23, 529
- [75] Stokes R.A., Partridge R.B., Wilkinson D.T. 1967, Phys. Rev. Lett., 19, 1199
- [76] Toffolatti L. & De Zotti G. 1988, private communication
- [77] Waters J.W. 1976 in Method of Experimental Physics, ed M. L. Meeks (New York: Academic), 12B, 142
- [78] Welch W.J. et al. 1967, Phys. Rev. Lett., 18, 1068
- [79] Wilkinson D.T. 1967, Phys. Rev. Lett., 19, 1195

Figure 1: Galactic emission components and CMB spectra for moderate angular resolution (7° HPBW) and galactic latitude $|b| < 20^\circ$. The shaded regions indicate the range of synchrotron, free-free and dust emission. Solid lines indicate the mean CMB spectrum and rms amplitude of anisotropy (from Platania et al. 1998).

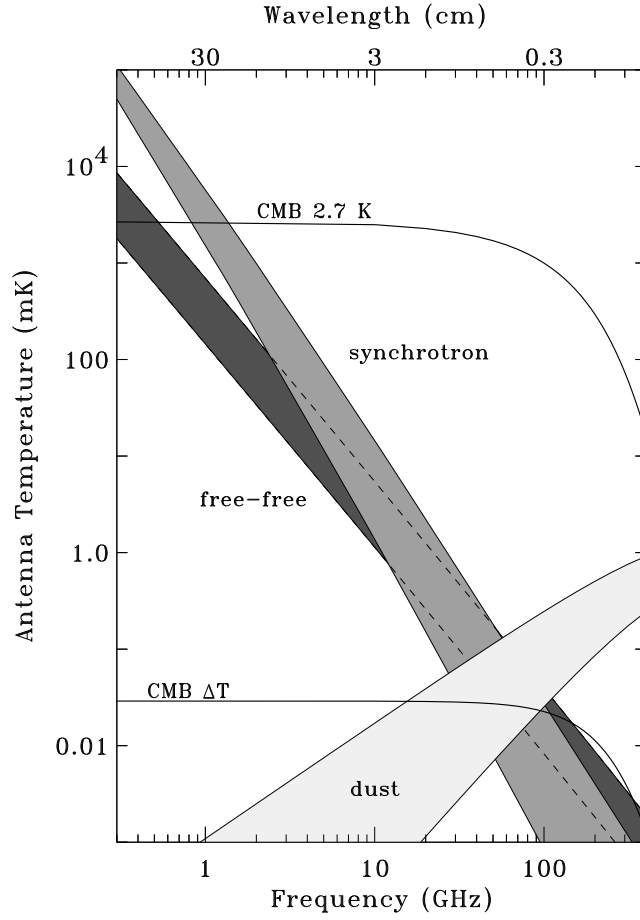


Figure 2: Comparison between the measures of the $T_{CMB}(z)$ and the scale-law of equation (24)(solid line). Figure from Ge et al. 1995

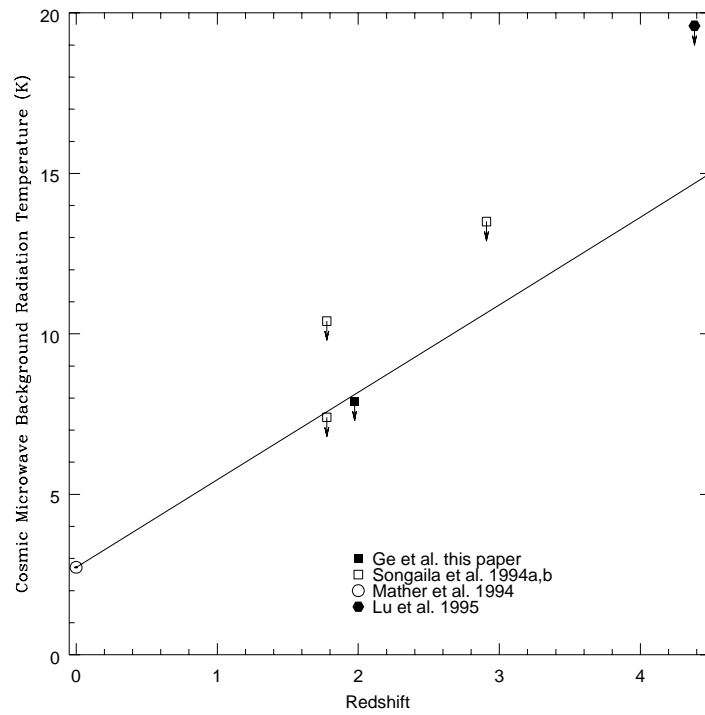


Figure 3: Plot of all measures of the CMB thermodynamic temperature. The big stars are the early ground measurements, the small stars the recent ground measurements, the squares the balloon measurements, the triangles the experiments with the CN molecular and the diamonds the COBRA data. The FIRAS data are plot as a solid line.

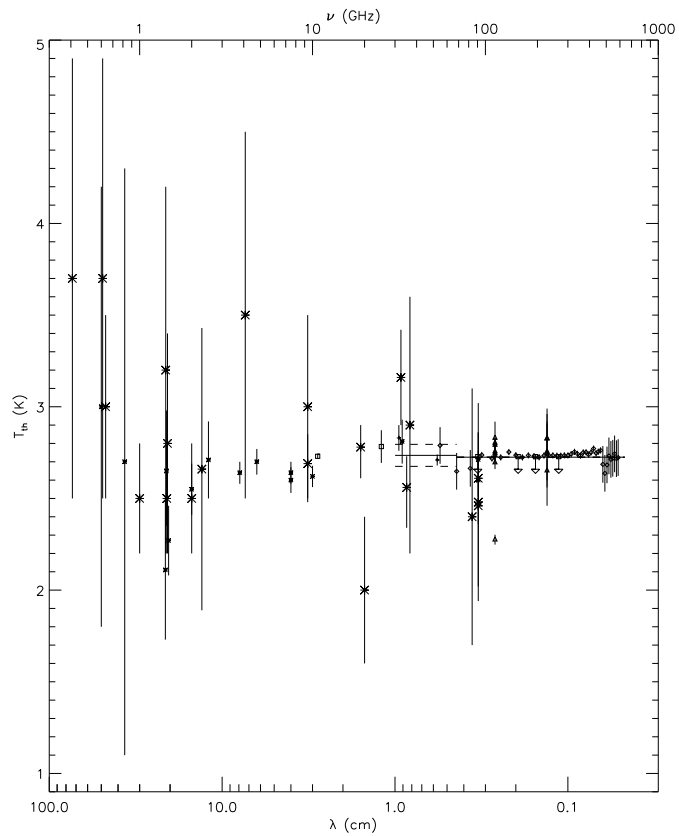


Figure 4: Plot of the more recent measures of the CMB thermodynamic temperature. The small stars the recent ground measurements, the squares the balloon measurements, the triangles the experiments with the CN molecular and the diamonds the COBRA data. The FIRAS data are plot as a solid line.

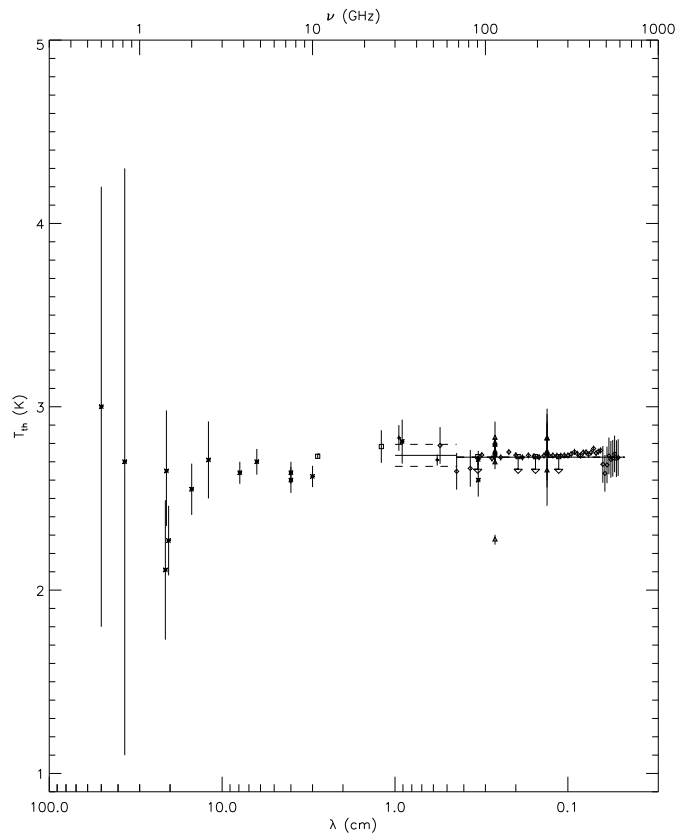
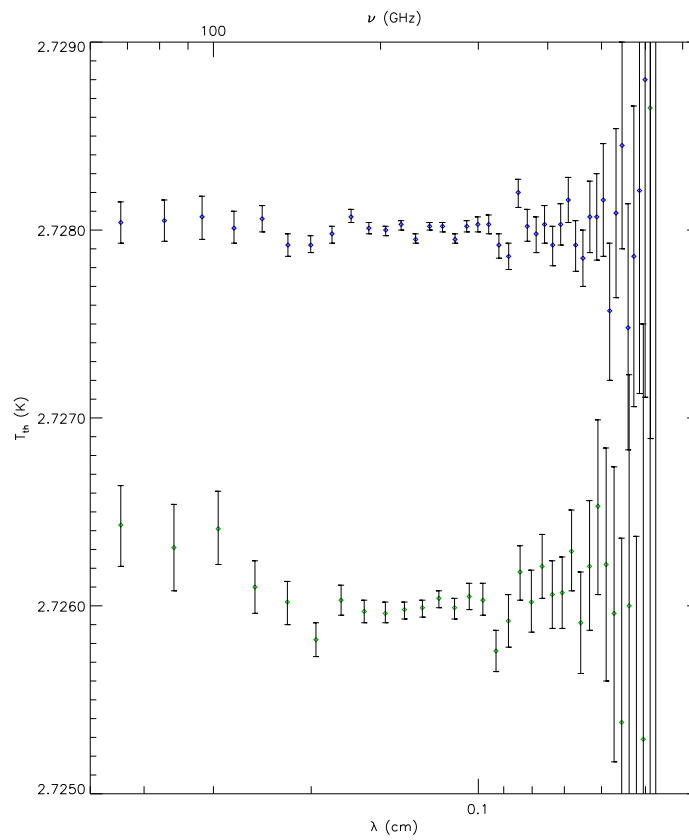


Figure 5: A comparison between the FIRAS data reported by Mather et al. (1994) and the more refined analysis of these by Fixsen et al. (1996)



Frequency cm^{-1}	Residual kJy/sr	Uncertainty 1σ	Astrophysical monopole
2.27	5	14	4
2.72	9	19	3
3.18	15	25	-1
3.63	4	23	-1
4.08	19	22	3
4.54	-30	21	6
4.99	-30	18	8
5.45	-10	18	8
5.90	32	16	10
6.35	4	14	10
6.81	-2	13	12
7.26	13	12	20
7.71	-22	11	25
8.17	8	10	30
8.62	8	11	36
9.08	-21	12	41
9.53	9	14	46
9.98	12	16	57
10.44	11	18	65
10.89	-29	22	73
11.34	-46	22	93
11.80	58	23	98
12.25	6	23	105
12.71	-6	23	121
13.16	6	22	135
13.61	-17	21	147
14.07	6	20	160
14.52	26	19	178
14.97	-12	19	199
15.43	-19	19	221
15.88	8	21	227
16.34	7	23	250
16.79	14	26	275
17.24	-33	28	295
17.70	6	30	312
18.15	26	32	336
18.61	-26	33	363
19.06	-6	35	405
19.51	8	41	421
19.97	26	55	435
20.42	57	88	477
20.87	-116	155	519
21.33	-432	282	573

Table 16: Monopole spectrum (Fixsen et al. 1996)

ν (GHz)	T_{CMB}^{th} (K)	Upper error (K)	Lower error (K)
68.1	2.72804	.00011	.00011
81.5	2.72805	.00011	.00011
95.3	2.72807	.00011	.00011
108.8	2.72801	.00009	.00009
122.3	2.72806	.00007	.00007
136.1	2.72792	.00006	.00006
149.6	2.72792	.00005	.00005
163.4	2.72798	.00004	.00004
176.9	2.72807	.00004	.00004
190.4	2.72801	.00003	.00003
204.2	2.72800	.00003	.00003
217.6	2.72803	.00002	.00002
231.1	2.72795	.00002	.00002
244.9	2.72802	.00002	.00002
258.4	2.72802	.00002	.00002
272.2	2.72795	.00003	.00003
285.7	2.72802	.00003	.00003
299.2	2.72803	.00004	.00004
313.0	2.72803	.00005	.00005
326.5	2.72792	.00006	.00006
340.0	2.72786	.00007	.00007
353.8	2.72820	.00008	.00008
367.2	2.72802	.00008	.00008
381.0	2.72798	.00009	.00009
394.5	2.72803	.00010	.00010
408.0	2.72792	.00010	.00010
421.8	2.72803	.00011	.00011
435.3	2.72816	.00012	.00012
448.8	2.72792	.00013	.00013
462.6	2.72785	.00015	.00015
476.1	2.72807	.00019	.00019
489.9	2.72807	.00023	.00023
503.4	2.72816	.00030	.00030
516.8	2.72757	.00037	.00037
530.6	2.72809	.00045	.00045
544.1	2.72845	.00055	.00055
557.9	2.72748	.00066	.00066
571.4	2.72786	.00080	.00080
584.9	2.72821	.00108	.00108
598.7	2.72880	.00168	.00168
612.2	2.73002	.00311	.00311
625.7	2.72316	.00652	.00652
639.5	2.70634	.01468	.01468

Table 17: Value and statistical error of the CMB temperature for each FIRAS channel (Nordberg & Smoot 1998)

	Fit Value	Statistical uncertainty (1σ)	Systematic uncertainty (1σ)	Final uncertainty (1σ)
Galaxy Temp	13.3	0.6	0.8	1.0 K
Dipole Amp	3.372	0.004	0.006	0.007 mK
Dipole Temp	2717	3	6	7 mK
Gal Latitude	48.26	0.11	0.10	0.15 deg
Gal Longitude	264.14	0.14	0.06	0.15 deg
CMBR Temp	2.728	0.00001	0.002	0.002 K

Table 18: Fit results (Fixsen et al. 1996)

ν (GHz)	T_{CMB}^{th} (K)	Upper error (K)	Lower error (K)
54.6	2.789	.100	.100
68.1	2.648	.100	.100
81.8	2.664	.100	.100
95.3	2.737	.010	.010
109.1	2.718	.010	.010
122.6	2.724	.010	.010
136.4	2.753	.010	.010
149.9	2.736	.010	.010
163.7	2.724	.010	.010
177.2	2.735	.010	.010
191.0	2.731	.010	.010
204.5	2.725	.010	.010
218.2	2.734	.010	.010
231.7	2.737	.010	.010
245.5	2.735	.010	.010
259.0	2.733	.010	.010
272.8	2.733	.010	.010
286.3	2.735	.010	.010
300.1	2.735	.010	.010
313.6	2.742	.010	.010
327.4	2.754	.010	.010
340.9	2.743	.010	.010
354.7	2.734	.010	.010
368.1	2.751	.010	.010
381.9	2.752	.010	.010
395.4	2.739	.010	.010
409.2	2.752	.010	.010
422.7	2.772	.010	.010
436.5	2.747	.010	.010
450.0	2.755	.010	.010
463.8	2.762	.010	.010
477.3	2.686	.100	.100
491.1	2.637	.100	.100
504.6	2.683	.100	.100
518.3	2.732	.100	.100
531.8	2.713	.100	.100
545.6	2.719	.100	.100
559.1	2.743	.100	.100
572.9	2.717	.100	.100
586.4	2.723	.100	.100

Table 19: Value and error of the CMB temperature for each COBRA channel (Nordberg & Smoot 1998)

Value	Meaning
0	the statistical error is on the total
1	the statistical error is on one of the terms that give the total error. This is also a lower limit for this value
2	the statistical error is extrapolated from the values of measurements in close frequencies
3	the statistical error is not known
4	we have no information on the errors. We assign the entire error to statistical source
5	COBRA problematical data: the total error is conservative. In the columns are given the errors reported by Gush et al. (1990)
6	FIRAS data from the first calibration (Mather et al. 1990)

Table 20: Meaning of the flag value